Journal of Pharmaceutical Analysis 15 (2025) 101054

Contents lists available at ScienceDirect

Journal of Pharmaceutical Analysis

journal homepage: www.elsevier.com/locate/jpa

Original article

Oxymatrine, a novel TLR2 agonist, promotes megakaryopoiesis and thrombopoiesis through the STING/NF-κB pathway

Chengyang Ni [a, 1], Ling Zhou [a, 1], Shuo Yang [a], Mei Ran [a], Jiesi Luo [b, c], Kui Cheng [d], Feihong Huang [a], Xiaoqin Tang [a], Xiang Xie [e], Dalian Qin [a], Qibing Mei [a], Long Wang [a, ***], Juan Xiao [f, **], Jianming Wu [b, c, *]

[a] Sichuan Key Medical Laboratory of New Drug Discovery and Druggability, Luzhou Key Laboratory of Activity Screening and Druggability Evaluation for Chinese Materia Medica, School of Pharmacy, Southwest Medical University, Luzhou, Sichuan, 646000, China
[b] School of Basic Medical Sciences, Southwest Medical University, Luzhou, Sichuan, 646000, China
[c] Education Ministry Key Laboratory of Medical Electrophysiology, Southwest Medical University, Luzhou, Sichuan, 646000, China
[d] Guangdong Provincial Key Laboratory of New Drug Screening and NMPA Key Laboratory for Research and Evaluation of Drug Metabolism, School of Pharmaceutical Sciences, Southern Medical University, Guangzhou, 510515, China
[e] Public Center of Experimental Technology, Model Animal and Human Disease Research of Luzhou Key Laboratory, School of Basic Medical Sciences, Southwest Medical University, Luzhou, Sichuan, 646000, China
[f] Department of Cardiovascular Medicine, The Affiliated Hospital of Southwest Medical University, Luzhou, Sichuan, 646000, China

ARTICLE INFO

Article history:
Received 3 February 2024
Received in revised form
17 July 2024
Accepted 22 July 2024
Available online 23 July 2024

Keywords:
Oxymatrine
Megakaryocyte differentiation
Thrombopoiesis
Platelets
Toll-like receptor 2

ABSTRACT

Radiation-induced thrombocytopenia (RIT) faces a perplexing challenge in the clinical treatment of cancer patients, and current therapeutic approaches are inadequate in the clinical settings. In this research, oxymatrine, a new molecule capable of healing RIT was screened out, and the underlying regulatory mechanism associated with magakaryocyte (MK) differentiation and thrombopoiesis was demonstrated. The capacity of oxymatrine to induce MK differentiation was verified in K-562 and Meg-01 cells *in vitro*. The ability to induce thrombopoiesis was subsequently demonstrated in Tg (cd41:enhanced green fluorescent protein (eGFP)) zebrafish and RIT model mice. In addition, we carried out network pharmacological prediction, drug affinity responsive target stability assay (DARTS) and cellular thermal shift assay (CETSA) analyses to explore the potential targets of oxymatrine. Moreover, the pathway underlying the effects of oxymatrine was determined by Kyoto Encyclopedia of Genes and Genomes (KEGG) enrichment analyses, Western blot (WB), and immunofluorescence. Oxymatrine markedly promoted MK differentiation and maturation *in vitro*. Moreover, oxymatrine induced thrombopoiesis in Tg (cd41:eGFP) zebrafish and accelerated thrombopoiesis and platelet function recovery in RIT model mice. Mechanistically, oxymatrine directly binds to toll-like receptor 2 (TLR2) and further regulates the downstream pathway stimulator of interferon genes (STING)/nuclear factor-kappaB (NF-κB), which can be blocked by C29 and C-176, which are specific inhibitors of TLR2 and STING, respectively. Taken together, we demonstrated that oxymatrine, a novel TLR2 agonist, plays a critical role in accelerating MK differentiation and thrombopoiesis via the STING/NF-κB axis, suggesting that oxymatrine is a promising candidate for RIT therapy.

1. Introduction

Cancer as a common cause of death worldwide, is characterized by multifactorial and complex mechanisms that are continually evolving [1,2]. Radiotherapy, a primary method for cancer treatment, still causes side effects such as damage to normal tissues, immunosuppression, and inhibition of myelopoiesis [3,4]. Hematopoietic stem cells (HSCs) can be destroyed after radiotherapy and eventually cause a variety of complications, including platelet depletion and immune dysfunction [4]. In addition, survival rates after total body irradiation are more closely associated with platelet counts than with other hematologic marker counts [5]. Platelets are tiny blood cells that are crucial for angiogenesis and inflammation and participate in clotting reactions [6]. Platelet dysfunction can cause petechiae and mucocutaneous bleeding [7]. Radiation-induced thrombocytopenia (RIT) is defined as a hematological

Peer review under responsibility of Xi'an Jiaotong University.
* Corresponding author. School of Basic Medical Sciences, Southwest Medical University, Luzhou, Sichuan, 646000, China.
** Corresponding author.
*** Corresponding author.
E-mail addresses: jianmingwu@swmu.edu.cn (J. Wu), xj5101465@swmu.edu.cn (J. Xiao), wanglongsdu1226@163.com (L. Wang).
[1] Both authors contributed equally to this work.

https://doi.org/10.1016/j.jpha.2024.101054

disease in which peripheral blood (PB) platelet counts are less than 100×10^9/L [8]. Platelet transmission has been utilized to cure severe thrombocytopenia, but it is associated with alloimmunization and nonhemolytic reactions [9]. Unfortunately, therapeutic agents, such as thrombopoietin (TPO) receptor agonists (TPO-RAs), cytokines, and corticosteroids, can cause adverse effects such as thromboembolic complications and unsatisfactory immunogenicity [10]. Hence, the treatment of thrombocytopenia requires the identification of alternative therapeutic compounds with high efficacy and low toxicity.

Platelets are anucleate cells that are the terminal product of megakaryocytes (MKs) differentiation and maturation [11]. As a product of HSC development, MKs undergo a continuous and intricate process of endomitosis and eventually mature [12]. Mature MKs are characterized by rapid DNA replication and cytoplasmic maturation without cell division [13] and release functional platelets into the bloodstream under the sheer force of blood flow [14,15]. Thrombopoiesis and maturation occur dynamically in MKs, and following these processes, MKs express several surface markers, including CD41 and CD42b [16]. In addition, the development of MKs and platelet production depend on the well-regulated cytoskeleton made of tubulin and actin [17]. Moreover, early growth response protein 1 (EGR1), runt-related transcription factor 1 (RUNX1), cellular oncogene fos (FOS), and nuclear factor erythroid 2 (NF-E2) are MK maturation-related transcription factors (TFs) that are essential for platelet production. Any MKs abnormality may cause platelet disorders due to the abnormal maturation and release of platelets [18].

The endoplasmic reticulum (ER) protein stimulator of interferon genes (STING) is a consensus transmembrane protein [19]. STING has been extensively studied recently, and its relationship with innate immunity has been highlighted in numerous reports. Initially, the STING pathway was found to be connected primarily to immune mechanisms in infectious diseases [20,21], but further investigations have revealed that the STING pathway is also involved in cancer and autoimmunity [22,23]. Interestingly, a recent research has been reported that the STING pathway regulates platelet activation and granule secretion [24]. However, how STING modulates MK differentiation and thrombopoiesis is a perplexing and equally interesting issue.

Toll-like receptor 2 (TLR2), a functional receptor involved in the activation of innate immunity, has been reported to be expressed in MKs and platelets [25]. Moreover, the receptor of TLR2 has been shown to regulate platelet formation through platelet aggregation, activation processes, and cooperation with leukocytes [26]. The signaling pathways activated by TLR2 include the mitogen-activated protein kinase (MAPK) pathway and nuclear factor-kappaB (NF-κB) pathway [27]. Primarily, the function of the TF NF-κB is to regulate transcription processes such as innate immunity and inflammation. Interestingly, NF-κB was reported to a play nongenomic role in platelet aggregation. Therefore, increasing interest in activating the TLR2/NF-κB pathway for the treatment of platelet function-related diseases has been revealed [28]. The relevance of STING activation to TLR2/NF-κB has been reported [29]. However, research on the correlation between platelet counts and TLR2/STING/NF-κB expression is quite limited, and further investigations are greatly needed [30].

Oxymatrine is a quinolizidine alkaloid with a unique architecture that is extracted from the roots of *Sophora flavescens* Ait. [31]. Oxymatrine possess multiple pharmacological effects, including antiviral, antifibrotic, and other immune-regulating effects [32,33]. However, the underlying mechanism by which oxymatrine exerts its pharmacological effects is still ambiguous. Interestingly, through our preliminary investigation of drug activity, oxymatrine appears to be able to induce megakaryopoiesis and thrombopoiesis.

In the present research, oxymatrine promoted MK differentiation *in vitro*, which was confirmed by the increase in cell size, increased expression of matural MK-specific markers, and increase in polyploidization. Subsequently, the effect of oxymatrine on thrombopoiesis was verified by using the Tg (cd41:eGFP) transgenic zebrafish model. A RIT model was subsequently established in mice, and the results showed that oxymatrine treatment markedly ameliorated thrombocytopenia in mice with acute irradiation injury. To investigate the underlying mechanism by which oxymatrine promotes MK differentiation, network pharmacology and Western blot (WB) were utilized, which demonstrated that oxymatrine targeted TLR2 and activated the downstream pathway of STING/NF-κB. Taken together, our research provides novel pharmacological insight into oxymatrine, which could lead to the use of oxymatrine as a potential drug for the clinical treatment of RIT.

2. Materials and methods

2.1. Chemicals

Oxymatrine (purity: 99.5%, as determined by high performance liquid chromatography (HPLC)) was obtained from Shanghai McLean Biochemical Technology Co., Ltd. (Shanghai, China). C29 (purity: 98%, as determined by HPLC), C-176 (purity: 99.45%, as determined by HPLC), and Pam3CSK4 (purity: 99.01%, as determined by HPLC) were purchased from MedChemExpress LLC (Herndon, VA, USA).

2.2. Cell culture

The American Type Culture Collection (ATCC; Manassas, VA, USA) supplied the K-562 human chronic myeloid leukemia cell line and Meg-01 human megakaryoblastic leukemia cell line. The present study involved the cultivation of cells via Roswell Park Memorial Institute (RPMI)-1640 medium (Thermo Fisher Scientific Inc., Waltham, MA, USA) supplemented with 10% (*V*/*V*) fetal bovine serum (Sperikon Life Science & Biotechnology Co., Ltd., Chengdu, China), 0.5% (*V*/*V*) 100 U/mL penicillin, and 0.5% (*V*/*V*) 100 μg/mL streptomycin (Beyotime Biotechnology, Chengdu, China). The sample was incubated at a temperature of 37 °C in an incubator with high humidity and 5% carbon dioxide.

2.3. Cell Counting Kit-8 (CCK-8) assay

Cellular proliferation was assessed utilizing a the CCK-8 (APExBIO Technology LLC, Shanghai, China) assay. Briefly, the cells were seeded and cultured in 96-well plates at an initial concentration of 5×10^3 per well and then incubated with or without oxymatrine (10, 20, and 40 μM) for the indicated days. Subsequently, 20 μL of CCK-8 reagent was added to every well, and the cell culture was maintained for a period of 2 h. Triplicates were performed for all experiments. An absorbance spectrophotometer (BioTek Instruments, Inc., Winooski, VT, USA) was used to measure the absorbance. Using the following formula, cell viability was calculated: cell viability (%) = cells treated/cells control × 100%.

2.4. Lactate dehydrogenase (LDH) assay

An initial cell density of 5×10^3 K-562 and Meg-01 cells was maintained during the incubation process, which was conducted in 96-well plates. The cells were incubated with or without oxymatrine (10, 20, and 40 μM) for the indicated days. An LDH assay kit (Beyotime Biotechnology) was used following the instructions provided by the manufacturer. An LDH assay was employed to quantify the LDH levels in different cell populations, which was

achieved by introducing a lysis solution, thereby inducing LDH release from the cells for a duration of 1 h. LDH reagents were introduced to every well to enable the enzymatic catalysis reaction. Thereafter, the spectrophotometric absorbance of the solutions was recorded at 490 nm and 600 nm using a spectrophotometer (BioTek Instruments, Inc.).

2.5. Morphological analysis

K-562 and Meg-01 cells were seeded in a six-well plate at an initial density of 4×10^4 cells per well. Concurrently, the cells were treated with oxymatrine (10, 20, and 40 μM) or not for five days. The macroscopic marker of MK maturation is enlarged cell size, which is known as a MK-like change [34]. We observed the fields randomly and examined the morphology of mature cells that were two times larger than the morphology of undifferentiated cells via light microscopy (Nikon Corporation, Tokyo, Japan).

2.6. Giemsa staining

The morphology of the nucleus and cytoplasm was observed via Giemsa staining and visualized under a microscope [35]. K-562 and Meg-01 cells were seeded into six-well plates and subsequently incubated overnight in fresh complete medium. Then, the cellular specimens were treated with oxymatrine (10, 20, and 40 μM) in separate batches for five days. Finally, the cellular material was collected and subjected to two successive washes with phosphate-buffered saline (PBS). Subsequently, the cells were rendered immobile by means of a fixing solution comprising a mixture of methanol and glacial acetic acid at a 3:1 (*V*/*V*) ratio. A freshly prepared 5% Giemsa solution procured from Beijing Solarbio Science & Technology Co., Ltd. (Beijing, China) was introduced into the system, and the cells were subjected to a 15 min staining process at room temperature. The multiploid cells were photographed at 10× magnification under a microscope (Nikon Corporation).

2.7. Phalloidin staining

On the 5th day of treatment, the cells were acquired and subsequently placed on glass slides for F-actin staining utilizing the phalloidin staining methodology (Beijing Solarbio Science & Technology Co., Ltd.), which was carried out in compliance with the prescribed protocols of the manufacturer. Then, the cells were immobilized by means of a 4% solution of paraformaldehyde (Biosharp Life Sciences, Shanghai, China) for 15 min at ambient temperature and subsequently permeabilized utilizing a 0.05% Triton X-100 solution for 10 min. Following a washing step with PBS, a working solution of phalloidin conjugated with tetramethylrhodamine B isothiocyanate (TRITC) at a dilution ratio of 1:200 was applied to the glass slides harboring the cells. The cells were subsequently stained in the dark at ambient room temperature for 1 h. The cell nuclei were counterstained with 4′,6-diamidino-2-phenylindole (DAPI) (at concentration of 100 nM; Beijing Solarbio Science & Technology Co., Ltd.) for 30 s. The cells were observed under a laser scanning confocal microscope (Leica SP5 Microsystems GmbH, Wetzlar, Germany).

2.8. Immunofluorescence assay

After being treated with varying concentrations of oxymatrine (10, 20, and 40 μM) for five days, the cells were collected and fixed in a 4% paraformaldehyde fixative solution for 15 min. Subsequently, the cells were subjected to two rounds of washing with PBS. The cells were permeabilized with 0.05% Triton X-100 for 10 min at ambient temperature. After the addition of 5% bovine serum albumin (BSA), the cells were incubated at 4 °C overnight with anti-RUNX1 and anti-NF-E2 antibodies (Proteintech Group, Inc., Wuhan, China). After thorough washing with PBS, a fluorescent isothiocyanate-conjugated secondary antibody (Beijing Zhongshan Golden Bridge Biotechnology Co., Ltd., Beijing, China) was applied at a dilution of 1:100 to bind with the primary antibody. The nuclei were stained with DAPI. In the present investigation, an inverted fluorescence microscope (Nikon Corporation) was used to capture representative images.

2.9. Flow cytometry analysis of the MK differentiation markers CD41 and CD42b

For the flow cytometry analysis, 4×10^4 cells was seeded into six-well plates and treated with varying concentrations (10, 20, and 40 μM) of oxymatrine for five days. The cells were first collected and subsequently washed with ice-cold PBS. The cells were then treated with 8 μM fluorescein isothiocyanate (FITC)-conjugated anti-CD41 (Beijing 4A Biotech Co., Ltd., Beijing, China) and 8 μM phycoerythrin (PE)-conjugated anti-CD42b (Becton, Dickinson and Company, Franklin Lakes, NJ, USA) in 100 μL of PBS. The cellular suspension was subjected to a 30 min incubation period at a temperature of 4 °C in the dark. Subsequently, the suspended cells were subjected to analysis via resuspension in 400 μL of PBS on a FACSVerse flow cytometer (Becton, Dickinson and Company Biosciences, San Jose, CA, USA) resuspension in 400 μL of PBS. The proportion of cells expressing $CD41^+/CD42b^+$ was quantified.

2.10. Flow cytometry analysis of MK ploidy status

The cells were exposed to oxymatrine at concentrations of 10, 20, and 40 μM for five days. Subsequent to this intervention, the cells were procured and subjected to ploidy evaluation via the use of the CycleTEST™ PLUS DNA Reagent Kit (Becton, Dickinson and Company Biosciences) in strict accordance with the guidelines provided by the manufacturer. Briefly, the cellular specimens were subjected to a 10 min period of incubation with trypsin buffer, after which they received supplementary treatment with a trypsin inhibitor and ribonucleases (RNase) buffer for an additional 10 min. Next, the cells were incubated with a propidium iodide (PI) staining solution in the dark for 10 min. The identification of the samples was conducted through the use of a BD FACSCanto II flow cytometer (Becton, Dickinson and Company Biosciences). Finally, the data were analyzed using FlowJo software.

2.11. Cell apoptosis assay

Following a five-day treatment regimen with varying concentrations (10, 20, and 40 μM) of oxymatrine, a cytometry analysis utilizing an Annexin V-FITC/PI apoptosis detection kit (Vazyme Biotech (Nanjing) Co., Ltd., Nanjing, China) was performed to assess cell apoptosis. The cells were obtained and subjected to two cycles of rinsing with ice-cold PBS. Then, 100 μL of binding buffer solution was added to the cellular suspensions, and Annexin V-FITC and PI were added to the mixture following the manufacturer's instructions. Cellular apoptosis was subsequently assessed with a FACSVerse flow cytometer (Becton, Dickinson and Company Biosciences). The data acquisition and analysis procedure were performed utilizing FlowJo software (Becton, Dickinson and Company Biosciences).

2.12. Hoechst 33342 and PI costaining

The experimental procedure entailed the seeding of 4×10^4 cells per well into six-well plates, followed by the administration of oxymatrine at concentrations of 10, 20, and 40 μM for five days. The

cells were centrifuged at a speed of 1,500 rpm for 5 min and subsequently rinsed twice with PBS. A Hoechst 33342/PI kit (Beijing Solarbio Science & Technology Co., Ltd.) was used to assess apoptotic cell morphology following the manufacturer's instructions. Apoptotic cells that displayed morphological characteristics, such as chromosome aggregation, nuclear division, and nuclear fragmentation according to fluorescence microscopy, were identified and counted. Red and blue hyperfluorescence could be observed in necrotic cells.

2.13. Zebrafish experiments

The Tg (cd41:eGFP) zebrafish strain was acquired from the China Zebrafish Resource Center (CZRC; Shanghai, China) and maintained within the public platform of zebrafish technology at Southwest Medical University (Luzhou, China). Embryos were collected from naturally spawning plants and raised at 28.5 °C in Daniel's buffer supplemented with 0.05 mM/L 1-phenyl-2-thiourea (PTU) at 12 h post fertilization. Tg (cd41:eGFP) transgenic zebrafish larvae at 3 days post fertilization (dpf) were seeded in six-well plates (40 larvae in each plate) and treated with oxymatrine (10, 20 and 40 μM). At 5 dpf, the zebrafish larvae were embedded in agarose on glass slides for imaging under an Olympus Stereo microscope (Olympus Corporation, Tokyo, Japan). Images were processed with FIJI software.

2.14. Establishment of a thrombocytopenia mouse model

Kunming (KM) mice that were specific pathogen free (SPF), eight to ten weeks of age, and between 18 and 22 g were used in this study. These mice were acquired from Tengxin Biotechnology Co., Ltd. (Chongqing, China). The mice were housed under standard conditions, consisting of controlled temperature (22 ± 2 °C), humidity (55% ± 5%), and a balanced light/dark cycle of 12 h. The mice were provided unrestricted access to both commercially available standard food and purified drinking water. The laboratory Animal Ethics Committee of Southwest Medical University (Luzhou, China) authorized the experimental procedures in compliance with the ethical guidelines for animal experimentation (Approval No.: 20230802-001). After a period of acclimation for seven days, the animals were subjected to random allocation into four distinct groups: the control (normal) group, X-ray irradiation group characterized by the induction of thrombocytopenia, the X-ray + TPO-positive group (3000 U/kg), and finally the oxymatrine group. Excluding the normal control cohort, the remaining cohort of mice was exposed to a single dose of 4 Gy radiation to induce experimental hematopoietic dysfunction. Both the control group and model group underwent intraperitoneal injections of normal saline (0.1 mL per 10 g weight) over a period of 12 consecutive days. The remaining groups were intraperitoneally injected with TPO or oxymatrine (20 mg/kg) for 12 consecutive days.

2.15. Routine hematological analysis

Briefly, 40 μL of BP was obtained from the fundus vein plexus on the specified day and subsequently mixed with 160 μL of diluent for blood cell analysis. In the present study, all samples were analyzed using an automated hematology analyzer (Sysmex Corporation, Kobe, Japan) to determine blood cell counts.

2.16. Histology analysis

Three mice from each designated cohort were randomly selected, and following a 12 days administration of oxymatrine, their femurs, lungs, kidneys, and livers were extracted for analysis. The samples were subjected to fixation using a 10% formaldehyde solution for one day. Thereafter, the femurs were decalcified using a decalcifying solution for one month. The organs were embedded in paraffin and prepared into sections with a thickness of 5 μm. The sections were deparaffinized, stained with hematoxylin and eosin (H&E), and subsequently analyzed using an Olympus BX51 microscope manufactured by Olympus Corporation. The visual fields of each specimen were randomly captured, and the number of MKs was tallied.

2.17. Flow cytometry analysis of MK differentiation in bone marrow (BM) and spleen cells

Mouse BM cells from mice were effectively flushed from the mouse femurs using a syringe with saline solution. The spleens were ground and a cell suspension was obtained. These cells were subsequently carefully sieved through a fine-grade 200-mesh nylon net. The BM and spleen specimens were treated with red blood cell (RBC) lysis buffer (Beijing 4A Biotech Co., Ltd.) at a low temperature to lyse RBCs. The cells were collected and counted to establish an appropriate cellular concentration of 1×10^6 cells per sample. The specimens were tagged with FITC-conjugated anti-CD41 from BioLegend, Inc. (San Diego, CA, USA), in addition to PE-conjugated anti-CD117 (c-Kit) and PE-conjugated anti-CD61, both from Becton, Dickinson and Company Biosciences, while being kept on ice for 30 min in the dark. Subsequently, the specimens were reconstituted in 1 mL of PBS for flow cytometry analysis. This was performed using a BD FACSCanto II flow cytometer (Becton, Dickinson and Company Biosciences).

2.18. Flow cytometry analysis of PB cells

40 μL sample of PB was acquired from the venous plexus. The solution was then mixed with 1 mL of citrate solution and 130 μL of a flow cytometric preservation solution to enable examination via flow cytometry. Subsequently, 1 mL of citrate solution and 130 μL of the same preservation solution were added for further examination by flow cytometry. The cells was subjected to two PBS washes prior to the addition of 0.5 μL of FITC-conjugated anti-CD41, 1.25 μL of PE-conjugated anti-CD61, and 0.5 μL of FITC-conjugated anti-CD41 according to the manufacturer's recommendations. After being incubated for 15 min at ambient room temperature, the cells were resuspended in 400 μL of PBS. Next, the samples were evaluated using a BD FACSCanto II flow cytometer (Becton, Dickinson and Company Biosciences).

2.19. Platelet isolation and preparation

Mouse blood was collected in tubes filled with an anticoagulant solution comprising 3.8% sodium citrate at a volumetric ratio of 1:9. The procedure for the isolation of platelet-rich plasma (PRP) involved subjecting the blood sample to centrifugation at a force of 100 *g* for a duration of 10 min at room temperature. Then, the PRP was subjected to centrifugation at a force of 400 *g* for 10 min to pellet of platelets. Following pipetting and removal of the supernatant, the platelet pellet was subjected to a double wash with PBS and was subsequently suspended in a modified Tyrode's buffer. Finally, the samples were allowed to rest at an ambient temperature lasting for 2 h before subsequent analyses.

2.20. Platelet activation assay

The isolated platelets were then used to investigate platelet activation. The platelets were subjected to agonist stimulation using adenosine diphosphate (ADP) (5 μM) while being maintained at room temperature. In the subsequent step, platelets in the resting

and active states were incubated with PE-conjugated anti-CD62P (BioLegend, Inc.) for a period of 30 min in the dark and were subsequently subjected to analysis via flow cytometry.

2.21. Tail bleeding time

The duration of tail bleeding was determined in accordance with previously established protocols [36]. First, the mice were administered pentobarbital (50 mg/kg). Two millimeters of the distal end of the tail was excised and promptly submerged in saline solution at 37 °C. The bleeding time was assessed by recording the time elapsed from the excision to the initial cessation of bleeding.

2.22. Carotid artery thrombosis model

In accordance with earlier literature [37], the carotid artery thrombosis model was created using $FeCl_3$. To initiate thrombus formation, the left carotid artery of nonanesthetized mice was exposed, and 3 mm × 1.0 mm pieces of filter paper soaked in a solution of 10% (*m*/*V*) $FeCl_3$ was placed on the exposed area for 3 min. After removal of the filter paper, the carotid artery was subjected to washing using PBS. Subsequently, blood flow was continuously monitored through the use of a vascular flow probe, which involved the deployment of a Transonic Model TS420 flowmeter (Transonic Systems Inc., Ithaca, NY, USA).

2.23. Platelet aggregation assay

Using platelet-poor plasma prepared in accordance with the aforementioned methodology, PRP was procured via centrifugation at room temperature and speeds of 100 and 2,000 *g* for a duration of 10 min. The density of each sample was subsequently standardized to 300×10^9 by a hematology analyzer. Stimulation was induced by adding 200 μL of ADP (5 μM; Helena Laboratories Corporation, Beaumont, TX, USA), and platelet aggregation was subsequently measured utilizing a turbidimetric aggregation-monitoring device (Helena Laboratories Corporation). The referenced methodology was adopted from a prior publication [37].

2.24. Platelet adhesion assay

To prepare plates coated with collagen, 250 μL of 5 μg/mL collagen (manufactured by Helena Laboratories Corporation) was added to the bottom of each confocal dish, followed by an overnight incubation at 4 °C. The wells were treated with a 1% solution of BSA and then allowed to block for a period of 1 h at ambient temperature. Prior to this step, each well was thoroughly washed twice with PBS. PRP, at a density of 2×10^7 cells/mL, was added to each well and allowed to incubate at 37 °C for 45 min. The platelets were subsequently fixed with a 4% paraformaldehyde solution for 15 min and permeabilized with a 1% Triton X-100 solution for 10 min. In accordance with established laboratory protocols, the attached platelets were subjected to subsequent staining procedures utilizing a solution of TRITC-conjugated phalloidin (diluted to a ratio of 1:200). The staining process was completed utilizing an inverted fluorescence microscope manufactured by Nikon Corporation [38]. The average coverage of adhering platelets in the selected representative images was mapped through random capture and calculated using ImageJ software.

2.25. Target prediction

The structural information of oxymatrine was obtained from the PubChem database, and the related targets of the compound were acquired by entering its structural formula into the SwissTargetPrediction database [39]. To obtain other alternative targets of oxymatrine, we used the PharmMapper Platform based on a three-dimensional (3D) oxymatrine structure. The gene targets that are associated with the activity of oxymatrine were identified as drug targets, and no repeated or nonhuman sources were used. The present investigation identified “disease targets” relevant to thrombocytopenia from the GeneCards and DisGeNET databases while undertaking measures to remove duplicate occurrences [40]. Ultimately, the process of matching “drug targets” with “disease targets” resulted in the discovery of targets involved the treatment of RIT by oxymatrine.

2.26. Protein-protein interaction (PPI) network construction and screening of hub genes

To evaluate the interplay among the designated targets, the provided information pertaining to the common targets was uploaded to the STRING_v11.0 repository with the species classification denoted as “Homo sapiens”. Subsequently, the PPI network was constructed with the Search Tool for the Retrieval of Interacting Genes/Proteins (STRING) database, subsequently visualized and subjected to topological analysis using Cytoscape_v3.7.1 software [41]. The criteria employed in the identification of hub targets for oxymatrine in thrombocytopenia involved the analysis of interconnective nodes. Specifically, hub targets were determined based on the degree values that surpassed the corresponding medians, as well as the betweenness centrality and closeness centrality values that exceeded twice the corresponding medians.

2.27. Kyoto Encyclopedia of Genes and Genomes (KEGG) pathway enrichment analyses

The primary aim of the KEGG enrichment analysis is to elucidate genes that are differentially expressed and to identify the potentially involved pathways. The gene symbols associated with the prevalent targets were incorporated into the Database for Annotation, Visualization, and Integrated Discovery (DAVID)_v6.8, which contains inclusive KEGG gene sets. To uncover the fundamental mechanism driving the recovery from thrombocytopenia induced by oxymatrine, a KEGG analysis was conducted to screen potential pathways related to the target protein. The pathway enrichment analyses were processed for graphic representation via a bubble plot using the OmicShare platform.

2.28. Molecular docking simulation

The 3D configuration of oxymatrine was obtained from the PubChem database. The crystallographic structure of the TLR2 hub target was obtained from the Protein Data Bank maintained by the Research Collaboratory for Structural Bioinformatics (RCSB). Subsequently, all ligands cocrystallized with the TLR2 protein were extracted, followed by the removal of water molecules from the protein structure after evaluation of the X-ray diffraction patterns. Ultimately, the incorporation of hydrogen atoms into the protein framework was achieved, and virtual visualization of oxymatrine-protein interactions was performed through the utilization of the Surflex-Dock (SFXC) docking mode after protein structure preparation. The binding affinities are represented by the SFXC scores (total scores).

2.29. WB assay

The proteins of Meg-01 cells subjected to varying concentrations of oxymatrine were extracted and lysed with 1× radioimmune precipitation assay (RIPA) lysis buffer (Cell Signaling Technology,

Danvers, MA, USA) kept at low temperature. Protease inhibitors (Sigma-Aldrich Corporation, St. Louis, MO, USA) and phosphatase inhibitors (F. Hoffmann-La Roche Ltd., Penzberg, Germany) were added to the lysis buffer during the extraction process. The quantification of protein was conducted with the ues of the Quick Start™ Bradford 1× Dye Protein Assay Reagent (Bio-Rad Laboratories, Inc., Hercules, CA, USA). For the immunoblot analysis, protein samples were loaded onto 10% sodium dodecyl sulfate (SDS)-polyacrylamide gel electrophoresis (PAGE) gels at equimolar concentrations and subsequently transferred onto polyvinylidene fluoride (PVDF) membranes obtained from Bio-Rad Laboratories, Inc.. The membrane was blocked by adding a solution of 10% (*m*/*V*) skim milk for 1 h. Then, primary antibodies were introduced into the membrane, followed by incubation with horseradish peroxidase (HRP)-conjugated secondary antibodies (Cell Signaling Technology) for identification. The detection of protein bands was accomplished with the UltraSignal Hypersensitive ECL Chemiluminescence Substrate Kit, which was provided by Beijng 4A Biotech Co., Ltd.. These bands were subsequently visualized using the ChemiDoc MP Imaging System, which was manufactured by Bio-Rad Laboratories, Inc.. To quantify the results, ImageJ software developed by National Institutes of Health (Bethesda, MD, USA) was used. The PVDF membranes were subjected to antibody probing using the following antibodies: TLR2 (TU362792S; Abmart (Shanghai) Co., Ltd., Shanghai, China), p-STING (TA7416S; Abmart (Shanghai) Co., Ltd.), STING (TD12090S; Abmart (Shanghai) Co., Ltd.), p-inhibitory subunit of nuclear factor kappa B alpha (p-IκBα) (2589; Cell Signaling Technology), IκBα (4814; Cell Signaling Technology), p-NF-κB (3033; Cell Signaling Technology), NF-κB (10745-1-AP; Proteintech Group, Inc., Chicago, IL, USA), EGR1 (22008-1-AP; Proteintech Group, Inc.), FOS (ab11959; Abcam plc, Cambridge, UK), NF-E2 (11089-1-AP; Proteintech Group, Inc.), RUNX1 (25315-1-AP; Proteintech Group, Inc.), and glyceraldehyde-3-phosphate dehydrogenase (GAPDH) (60004-1-lg; Proteintech Group, Inc.).

2.30. Drug affinity responsive target stability (DARTS) assay

Meg-01 cells were treated with RIPA lysis buffer on ice for 15 min to facilitate cell lysis. The resultant supernatant was acquired by centrifugation at 12,000 r/min for 15 min. The protein concentration was determined using the Bradford reagent, followed by dilution in PBS to achieve a concentration of 5 mg/mL. The samples were treated with oxymatrine or dimethyl sulfoxide (DMSO) (D8371; Sigma-Aldrich Corporation) under ambient conditions for a duration of 1 h. Subsequently, 5× loading buffer was added to each sample, which was subsequently boiled at 95 °C for 10 min. Subsequently, the samples underwent WB analysis.

2.31. Cellular thermal shift assay (CETSA)

Meg-01 cells were lysed as the DARTS assay metioned obove. Subsequently, the cell lysates were separated into two groups, respectively. One group was treated with oxymatrine (100 μM) for 1 h, while the other group was treated with DMSO. Then, the lysates of two groups were divided into eight groups with equal portions and heated at successively higher temperatures (37−72 °C) for 4 min. Subsequently, 5× loading buffer was added to each sample, which was subsequently boiled at 95 °C for 10 min. Finally, all asmples were taken to analyze the density of TLR2 protein by WB assay.

2.32. Statistical analysis

The data obtained throughout the course of this study are presented in accordance with established academic conventions as the mean ± the standard deviation (SD) and were analyzed using GraphPad Prism 8.0 software (GraphPad Software Inc., La Jolla, CA, USA). The experiments were carried out in triplicate, unless otherwise specified. The statistical significance of differences between groups was determined using analysis of variance (ANOVA) and the Tukey-Kramer method was used for post hoc analysis. For all incidences, a P value < 0.05 was considered as significant difference.

3. Results

3.1. Screening safe concentrations of oxymatrine for the treatment of K-562 and Meg-01 MKs

To determine the optimal concentration of oxymatrine needed to induce MK differentiation, an *in vitro* analysis was conducted utilizing the CCK-8 assay to measure the proliferation of K-562 and Meg-01 cells. The results indicated that the proliferation of these cells was significantly suppressed compared to that of the control group (Figs. 1A and B), which may be related to MK differentiation and maturation [42]. Subsequently, the LDH release of each oxymatrine concentration treated MKs was evaluated, which was demonstrated to be a significant indicator of cell membrane integrity and cell cytotoxicity [43]. The investigation revealed that there was no noteworthy difference in LDH release between the oxymatrine treated and control groups. These findings provide compelling evidence that MKs differentiation can be induced with oxymatrine (Figs. 1C and D). Next, we verified the ability of oxymatrine at 10, 20, and 40 μM to induce MK differentiation. Notably, phorbol 12-myristate 13-acetate (PMA; 0.8 nM), which is commonly used for MK differentiation, was used as a positive control drug [44]. In a randomized manner, fields were chosen for observation under a light microscope. Our results indicated that K-562 and Meg-01 cells treated with oxymatrine and PMA exhibited a larger population of cells exhibiting MK-like features, including a greater diameter and increased cell size, than did their counterparts in the control group (Fig. 1E). In summary, oxymatrine may be an active compound that inhibits MK proliferation and significantly promotes MK-like morphological changes.

3.2. Oxymatrine promotes typical MK differentiation in a concentration-dependent manner

Several distinctive features may be observed during the differentiation and maturation process of MKs. These include the phenomenon of polyploidization of nuclei and the appearance of particular surface antigens, namely, CD41 and CD42b, as well as the development of a demarcation membrane system (DMS) [45,46]. As a preliminary step, we examined the cell surface markers CD41 and CD42b in K-562 and Meg-01 cells using flow cytometry. The present study revealed a significant increase in $CD41^+/CD42b^+$ cells in the group treated with oxymatrine at concentrations of 10, 20, and 40 μM (Figs. 2A and B). Flow cytometry analysis of MK ploidy showed that cells treated with oxymatrine notably increased the percentage of total 4 N and ≥4 N ploidy in both K-562 and Meg-01 cells (Figs. 2C and D). The Giemsa staining assay further confirmed the increased nuclear-cytoplasmic ratio in the oxymatrine and PMA treated two cell lines, as well as the numerous deeply stained multilocal nuclei compared to the single nucleus of control cells (Fig. 2E). In addition, after five days of oxymatrine intervention, phalloidin staining showed that the cytoplasm of the drug-treated group was expanded and that the expression of F-actin aggregation, which is associated with proplatelet formation (PPF), was upregulated. Nuclear polyploidy in the drug-treated group was clearly visualized by DAPI staining, whereas in the control group, polyploidy was rarely observed (Figs. 2F and G). MK maturation and the formation of proplatelets are accompanied by

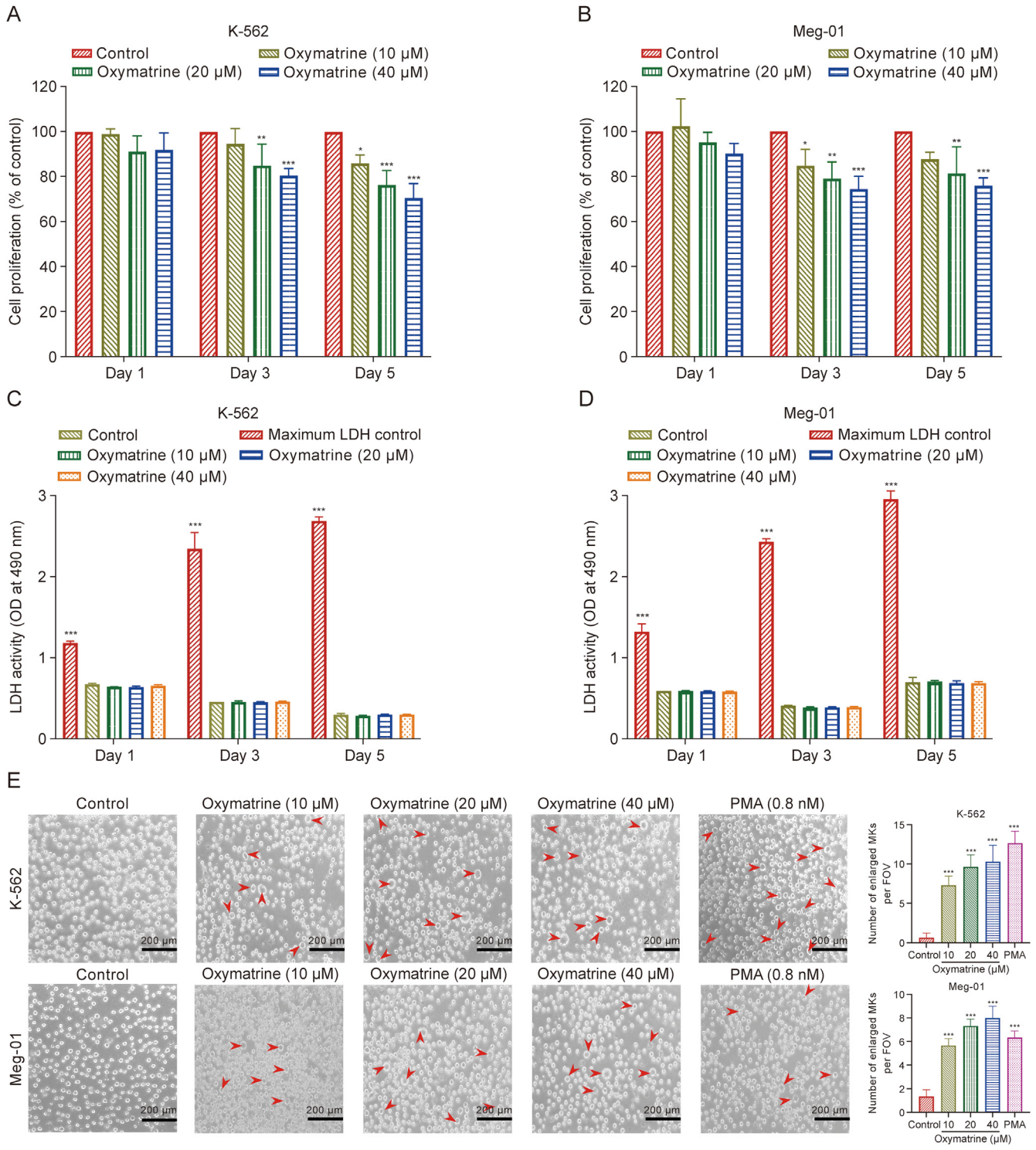

Fig. 1. Screening safe concentrations of oxymatrine for the treatment of K-562 and Meg-01 megakaryocyte (MK). (A, B) The Cell Counting Kit-8 (CCK-8) assay for oxymatrine-treated K-562 (A) and Meg-01 (B) MK proliferation. Three different time points and drug concentrations were used to measure the cell proliferation rate ($n = 6$ per group). (C, D) Detection of lactate dehydrogenase (LDH) release of K-562 (C) and Meg-01 (D) cells treated with different drug concentrations and measured at different time points ($n = 6$ per group). (E) Representative images of oxymatrine intervened K-562 and Meg-01 cells with various concentration (10, 20, and 40 μM) for five days ($n = 3$ per group). Phorbol 12-myristate 13-acetate (PMA) was used as positive control (0.8 nM). Data represent the mean ± standard deviation (SD) of six or three independent experiments and are analyzed by one-way analysis of variance (ANOVA) with Dunnett's 154. $^{*}P < 0.05$, $^{**}P < 0.01$, and $^{***}P < 0.001$ vs. the control. FOV: field of view.

cell apoptosis [47]. Here, the technique of flow cytometry was used to assess the impact of oxymatrine on apoptosis in K-562 and Meg-01 cells via Annexin V-FITC/PI costaining. After five days of oxymatrine treatment, cell apoptosis was induced in a concentration-dependent manner (Figs. S1A and B). Furthermore, the same drug-induced apoptosis was captured under a microscope by Hoechst 33343/PI costaining, but they were not present in the control group (Fig. S1C). Overall, the findings of this study have demonstrated that oxymatrine induces evident differentiation and maturation of MKs in a concentration-dependent manner.

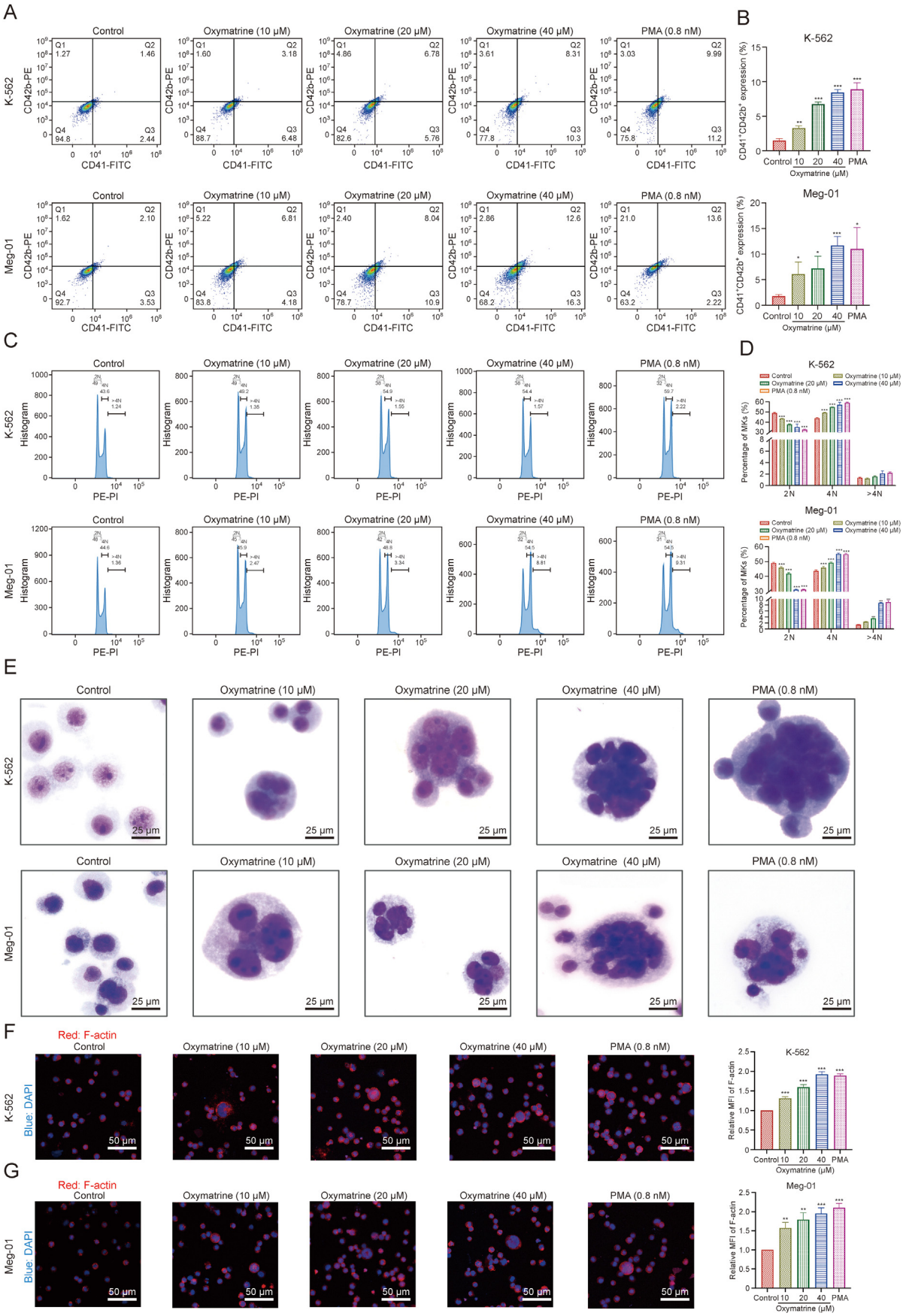

Fig. 2. Oxymatrine promotes typical megakaryocyte (MK) differentiation in concentration-dependent manner. (A) Analysis of $CD41^{+}/CD42b^{+}$ complex surface expression of oxymatrine (10, 20, and 40 μM) and phorbol 12-myristate 13-acetate (PMA; 0.8 nM) intervened K-562 and Meg-01 cell for five days by flow cytometry. (B) The percentage of $CD41^{+}/$

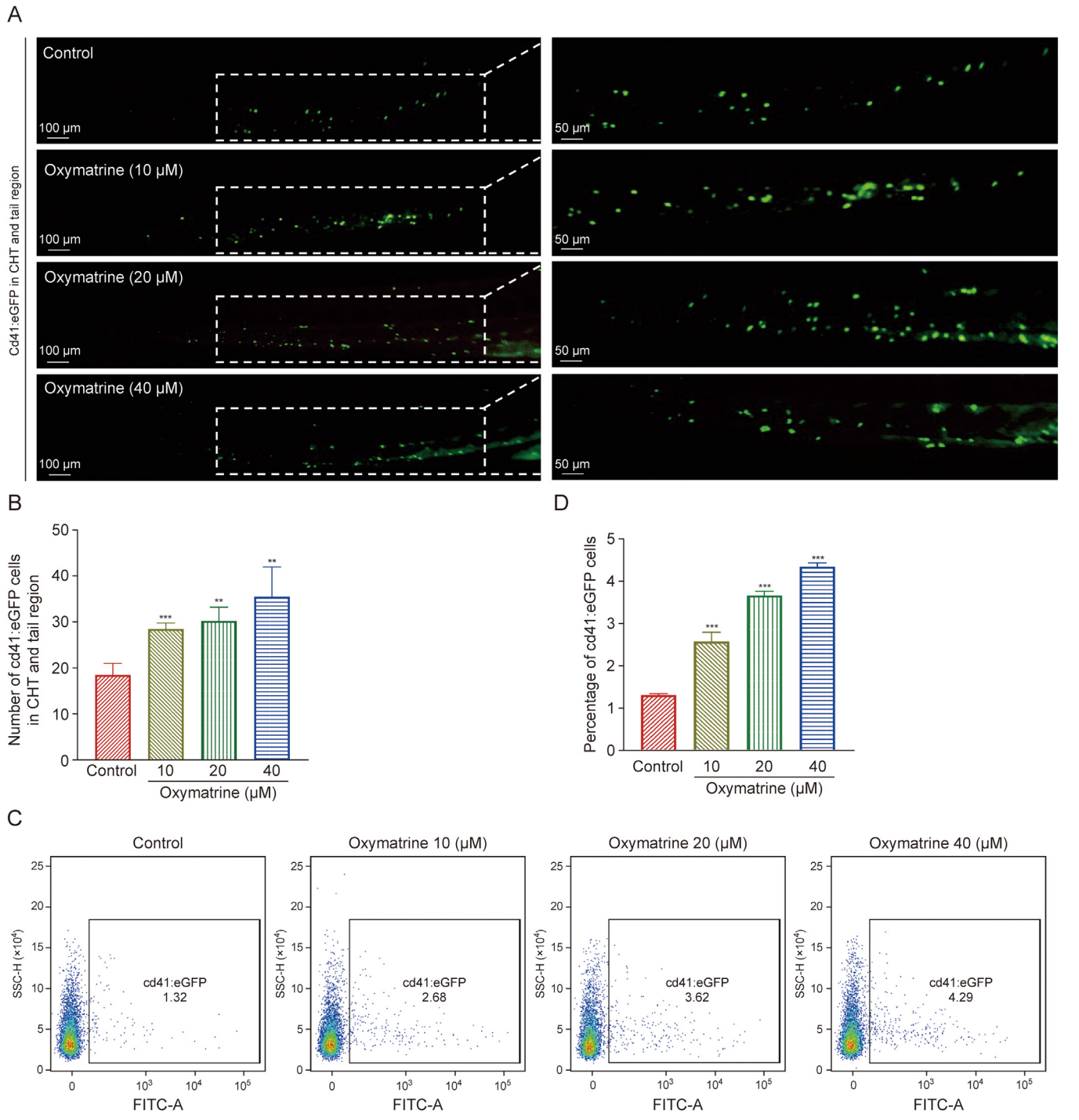

Fig. 3. Oxymatrine administration promotes thrombopoiesis in Tg (cd41:enhanced green fluorescent protein (eGFP)) transgenic zebrafish. (A) Cd41:eGFP$^+$ thrombocytes in the caudal hematopoietic tissue (CHT) region of oxymatrine (10, 20, and 40 μM) treated and control zebrafish. (B) Quantification of cd41:eGFP$^+$ cells in the CHT region in each group ($n = 4$ per group). (C) Flow cytometry analysis of cd41:eGFP$^+$ cells in zebrafish embryos. (D) Quantification of cd41:eGFP$^+$ cells in the zebrafish embryos in each group ($n = 3$ per group). Data represent the mean ± standard deviation (SD) of four or three independent experiments and are analyzed by one-way analysis of variance (ANOVA) with Dunnett's 154. $^{**}P < 0.01$, and $^{***}P < 0.001$ vs. the control. SSC: side scatter; FITC: fluorescein isothiocyanate.

CD42b$^+$ cells in the control and oxymatrine-treated groups ($n = 3$ per group). (C) The DNA ploidy analysis of oxymatrine (10, 20, and 40 μM) and PMA (0.8 nM) induced K-562 and Meg-01 cell for five days by flow cytometry. (D) The histogram represents the proportion of total 2 N, 4 N and ≥4 N ploidy in both K-562 and Meg-01 cells ($n = 3$ per group). (E) Giemsa staining of K562 and Meg-01 cells with or without oxymatrine (10, 20, and 40 μM) treatment for five days (PMA (0.8 nM) as positive control). (F, G) Phalloidin-labeled cytospin in K562 (F) and Meg-01 (G) cells intervened with multiple concentrations of oxymatrine (10, 20, and 40 μM) for five days under a fluorescence microscope ($n = 3$ per group). Excitation wavelength: 560 nm for phalloidin and 405 nm for 4′,6-diamidino-2-phenylindole (DAPI). Data represent the mean ± standard deviation (SD) of three independent experiments and are analyzed by one-way analysis of variance (ANOVA) with Dunnett's 154. $^{*}P < 0.05$, $^{**}P < 0.01$, and $^{***}P < 0.001$ vs. the control. FITC: fluorescein isothiocyanate; PE: phycoerythrin; PI: propidium iodide; MFI: mean fluorescence intensity.

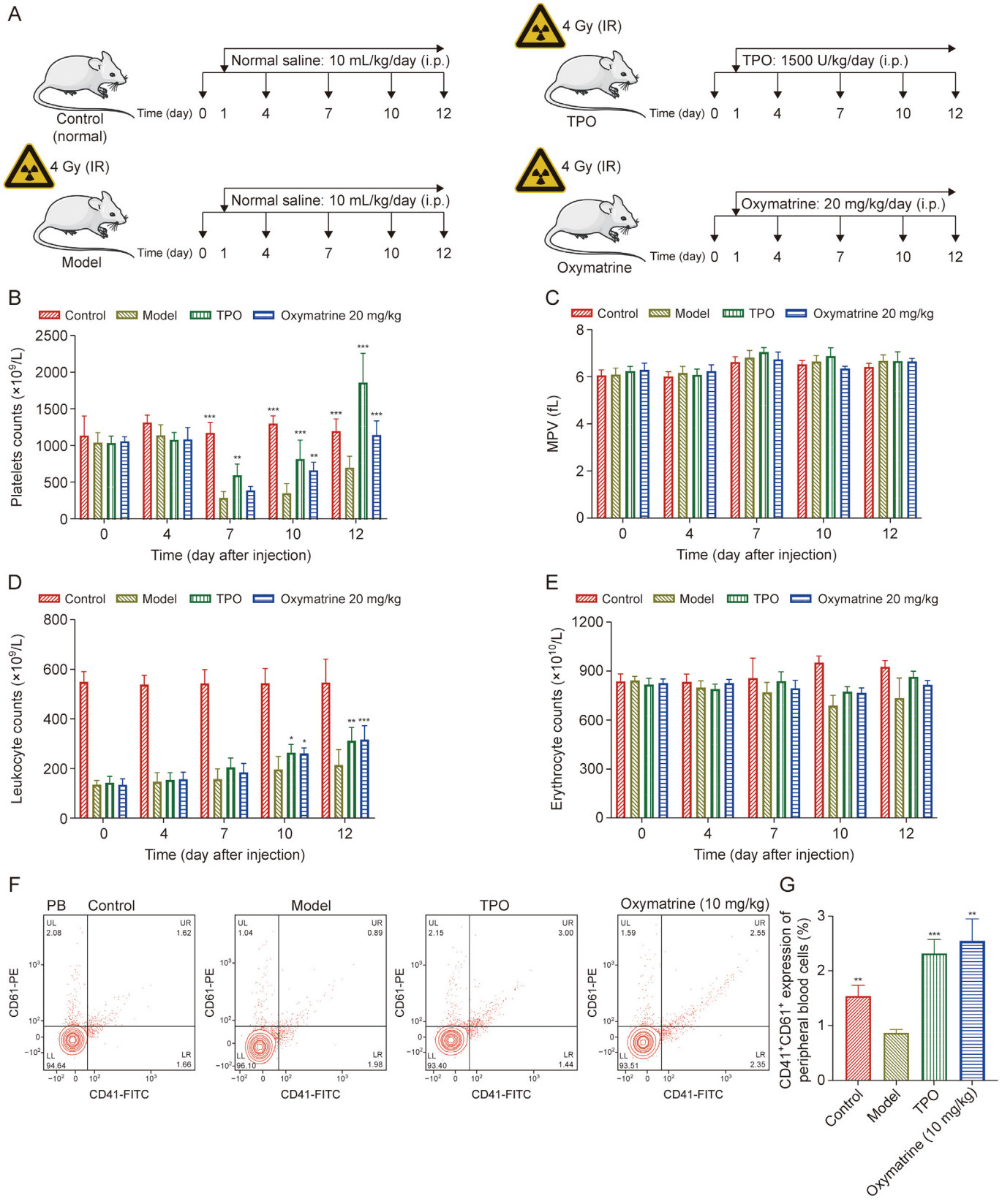

Fig. 4. Oxymatrine accelerates platelet recovery in acute X-ray irradiated mice. (A) The strategies of establishing the irradiated mice and treatment of each groups. (B) Peripheral platelet level of control group, thrombopoietin (TPO)-treated group (3000 U/kg), oxymatrine-treated group (20 mg/kg), and model group. Histology analysis was performed on days 0, 4, 7, 10, and 12 ($n = 6$ per group). (C) Mean platelet volume (MPV) values in each groups ($n = 6$ per group). (D) Leukocyte counts in each group ($n = 6$ per group). (E) Erythrocyte counts in each group ($n = 6$ per group). (F) Flow cytometry analysis of expression of CD41 and CD61 in peripheral blood (PB) platelets in each group after treatment for 12 days. (G) The histogram exhibits the percentage of expression of $CD41^+/CD61^+$ in PB cells in each group ($n = 3$ per group). Data represent the mean ± standard deviation (SD). Two-way analysis of variance (ANOVA) with Tukey's multiple comparisons test was used unless otherwise specified. $^*P < 0.05$, $^{**}P < 0.01$, and $^{***}P < 0.001$ vs. the corresponding model group. IR: ionizing radiation; FITC: fluorescein isothiocyanate; UL: upper left; UR: upper right; LL: lower left; LR: lower right.

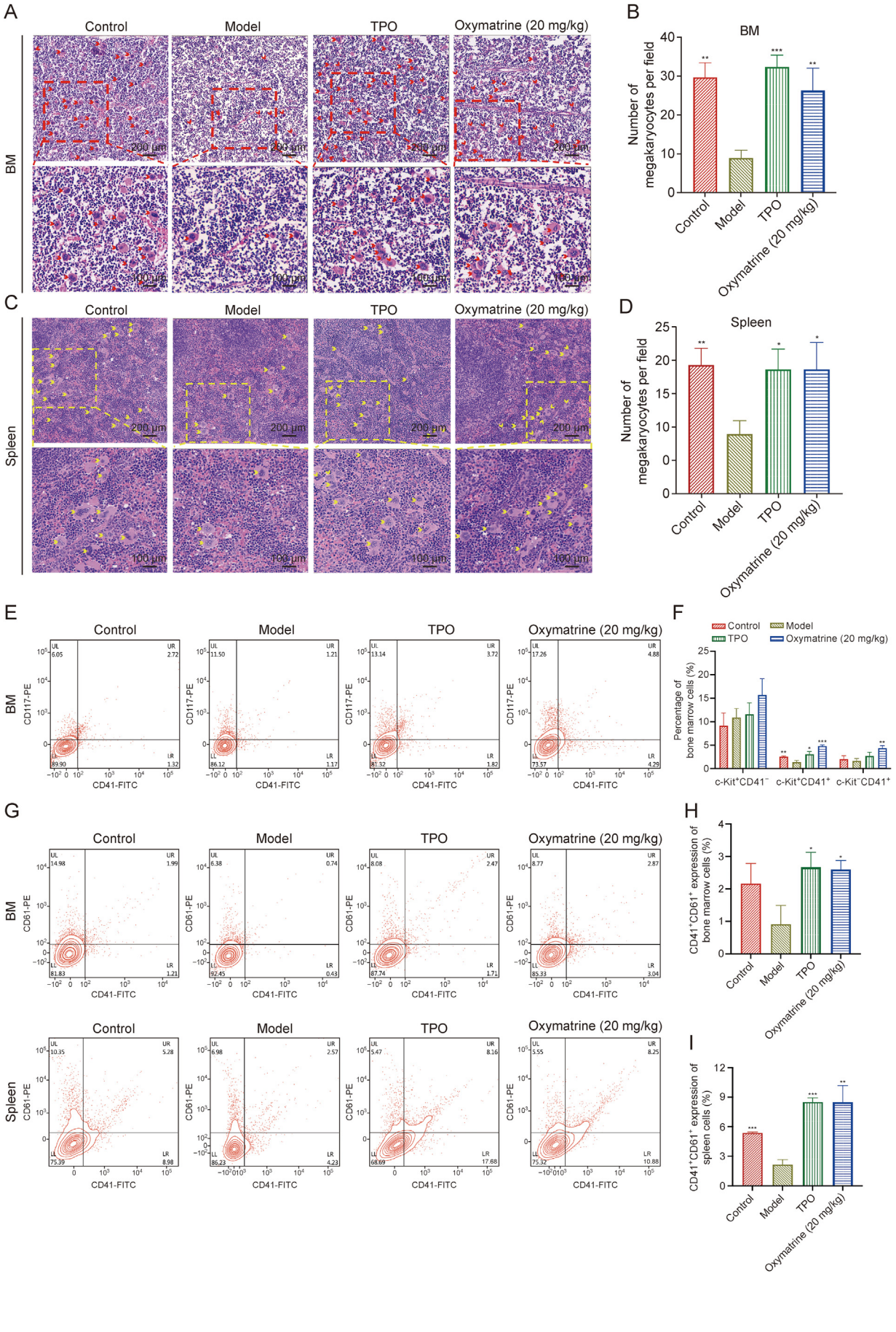
A
Control
Model
TPO
Oxymatrine (20 mg/kg)
BM
200 μm
100 μm
B
BM
Number of megakaryocytes per field
Control
Model
TPO
Oxymatrine (20 mg/kg)
C
Spleen
D
Spleen
E
CD117-PE
CD41-FITC
F
Percentage of bone marrow cells (%)
c-Kit+CD41−
c-Kit+CD41+
c-Kit−CD41+
G
CD61-PE
H
CD41+CD61+ expression of bone marrow cells (%)
I
CD41+CD61+ expression of spleen cells (%)

3.3. Oxymatrine promotes thrombopoiesis in zebrafish

To assess the capacity of oxymatrine to induce thrombopoiesis *in vivo*, zebrafish were used. At 3 dpf, Tg (cd41:eGFP) transgenic zebrafish were subjected to treatment with oxymatrine at various concentrations (10, 20, and 40 μM) (Fig. 3A). The results showed an increase in cd41:eGFP thrombocyte levels in the caudal hematopoietic tissue (CHT) region in the groups administered oxymatrine compared to those in the control group. Notably, the overall quantity of cd41:eGFP thrombocytes in the oxymatrine-treated groups was significantly greater than that in the control group (Fig. 3B). Moreover, we used flow cytometry to measure the percentage of cd41:eGFP positive cells among the zebrafish embryos (Fig. 3C), and the results showed that the ratio of cd41:eGFP cells was markedly increased after oxymatrine treatment (Fig. 3D). The results revealed that oxymatrine strongly enhanced thrombopoiesis in the zebrafish model.

3.4. Oxymatrine accelerates platelet recovery in acute X-ray irradiated mice

Drawing from the successful differentiation and maturation of MKs by oxymatrine *in vitro* and in zebrafish, our investigation aimed to evaluate the ability of oxymatrine to induce MK maturation *in vivo*, as this process precipitates thrombopoiesis in acute X-ray irradiated model mice. KM mice were exposed to systemic radiation at a single dose of 4.0 Gy, and subsequently administered with an intraperitoneal injection of oxymatrine at a dose of 20 mg/kg. The control and model groups were also administered with normal saline, while the positive control group was treated with TPO at a dose of 1500 U/kg. These interventions were performed consecutively for a duration of 12 days (Fig. 4A). The findings indicated that there was a decrease in the circulating platelet count among all groups of irradiated mice on the 7th day. Interestingly, no significant differences were observed when compared to those in the oxymatrine-treated group. Throughout the treatment course, it was observed that the TPO and oxymatrine treated cohorts experienced a significant increase in platelet count on days 10 and 12. These findings provide evidence suggesting that oxymatrine can stimulate thrombopoiesis (Fig. 4B). Mean platelet volume (MPV) is associated with platelet function and activation [48], and there was no significant difference among the groups, which suggested that the newly generated platelets induced by oxymatrine had no detrimental effects on platelet function (Fig. 4C). In addition, compared with those in the model group, the observed quantities of peripheral leukocytes and erythrocytes in both the oxymatrine and TPO administered groups were significantly greater (Figs. 4D and E). These findings indicate that oxymatrine may have the potential to mitigate radiation-induced myelosuppression and contribute to the restoration of blood levels. Subsequently, flow cytometry was used to evaluate the expression of CD41 and CD61 in cells present in the PB stream (Fig. 4F), which revealed that the percentage of $CD41^+/CD61^+$ cells in the oxymatrine treated group was markedly greater than that in the model group (Fig. 4G), which was in accordance with the increase in platelet count associated with oxymatrine treatment. Considering the implications for biological safety, an assessment was conducted on the hepatic tissue of mice through staining with H&E subsequent to treatment with oxymatrine. The findings demonstrated that there were no noteworthy pathological alterations observed in the entire hepatic lobule, and the fundamental configuration of hepatocytes centered around the central vein was conserved in all of the groups (Fig. S2). In summary, the findings presented above demonstrated that oxymatrine exerts a positive influence on the generation of platelets in murine models while simultaneously preventing any significant deleterious repercussions.

3.5. Oxymatrine rescues megakaryopoiesis in the BM and spleen after acute radiation injury

The predominant site of thrombopoiesis originating from MKs is within the BM, and its inhibition by ionizing radiation (IR) has been identified as a primary cause of hematopoietic injury. This condition is defined by the impairment of BM cellular structures. This phenomenon has been established through previous research [49]. The present study revealed significant disruption of the BM and vascular system in IR mice, characterized by substantial ablation of BM nucleated cells [50]. Moreover, physiological stress or disease can trigger extramedullary hematopoiesis (EMH) in the spleen, where BM hematopoiesis can be altered [51,52]. To evaluate alterations within the BM and spleen in response to a 12-day oxymatrine regimen, histological examination via H&E staining was carried out. The findings of the study revealed a noteworthy increase in the number of MKs within both the BM and spleen of the groups treated with oxymatrine and TPO in comparison to the model group. These outcomes strongly suggest that oxymatrine treatment effectively ameliorated the process of megakaryopoiesis in the BM and spleen (Figs. 5A–D). The present study subsequently assessed CD41 and c-Kit surface antigens in cells that were enriched in the BM. The present study demonstrated that the proportion of $c\text{-}Kit^+/CD41^-$ cells, which are hematopoietic progenitor cells, was not significantly different among the groups. However, the data revealed that the percentages of $c\text{-}Kit^+/CD41^+$ cells, which represent megakaryocytic progenitor cells, $c\text{-}Kit^-/CD41^+$ cells, or MK cells, were significantly greater in the oxymatrine-treated group than in the model group (Figs. 5E and F). This phenomenon can potentially be attributed to the BM cells being stimulated by oxymatrine, which leads to the transformation of immature $c\text{-}Kit^+/CD41^-$ cells into $c\text{-}Kit^+/CD41^+$ and mature $c\text{-}Kit^-/CD41^+$ (MK) cells. Subsequently, the cellular constituents of the BM and spleen were analyzed for the expression of the surface megakaryocytic markers CD41 and CD61. The present study revealed (Figs. 5G–I) that the proportion of $CD41^+/CD61^+$ cells in the oxymatrine and TPO-treated cohorts significantly increased compared to that in the model group, suggesting that oxymatrine induces the differentiation of MKs within the BM and spleen. The data obtained from the investigation revealed that the expression of hematopoietic surface markers was upregulated in response to oxymatrine treatment, indicating the maturation of MKs and the

Fig. 5. Oxymatrine rescues megakaryopoiesis in the bone marrow (BM) and spleen after acute radiation injury. (A) Representative images of hematoxylin and eosin (H&E) staining of BM from control group, model group, thrombopoietin (TPO)-treated (3000 U/kg) group, and oxymatrine-treated (20 mg/kg) group after treatment for 12 days. (B) The histogram exhibits the counts of BM megakaryocyte (MK) in each group ($n = 3$ per group). (C) Representative images of H&E staining of spleens from each group after treatment for 12 days. (D) The histogram shows the counts of spleen MKs in each group ($n = 3$ per group). (E) The analysis of $c\text{-}Kit^+/CD41^-$ (hematopoietic progenitor cells), $c\text{-}Kit^+/CD41^+$ (megakaryocytic progenitor cells), and $c\text{-}Kit^-/CD41^+$ (MKs) cell expression in each group after treatment for 12 days performed by flow cytometry. (F) The histogram exhibits the percentage of $c\text{-}Kit^+/CD41^-$, $c\text{-}Kit^+/CD41^+$, and $c\text{-}Kit^-/CD41^+$ cells in each group ($n = 3$ per group). (G) The expression of CD61 and CD41 in both BM MKs and spleen MKs was detected by flow cytometry after treatment for 12 days. (H) The histogram shows the percentage of $CD41^+/CD61^+$ cells in BM MKs of each groups ($n = 3$ per group). (I) The histogram shows the percentage of $CD41^+/CD61^+$ cells in spleen MKs of each group ($n = 3$ per group). Data represent the mean ± standard deviation (SD) of three independent experiments. $^*P < 0.05$, $^{**}P < 0.01$, and $^{***}P < 0.001$ vs. the model group. PE: phycoerythrin; FITC: fluorescein isothiocyanate; UL: upper left; UR: upper right; LL: lower left; LR: lower right.

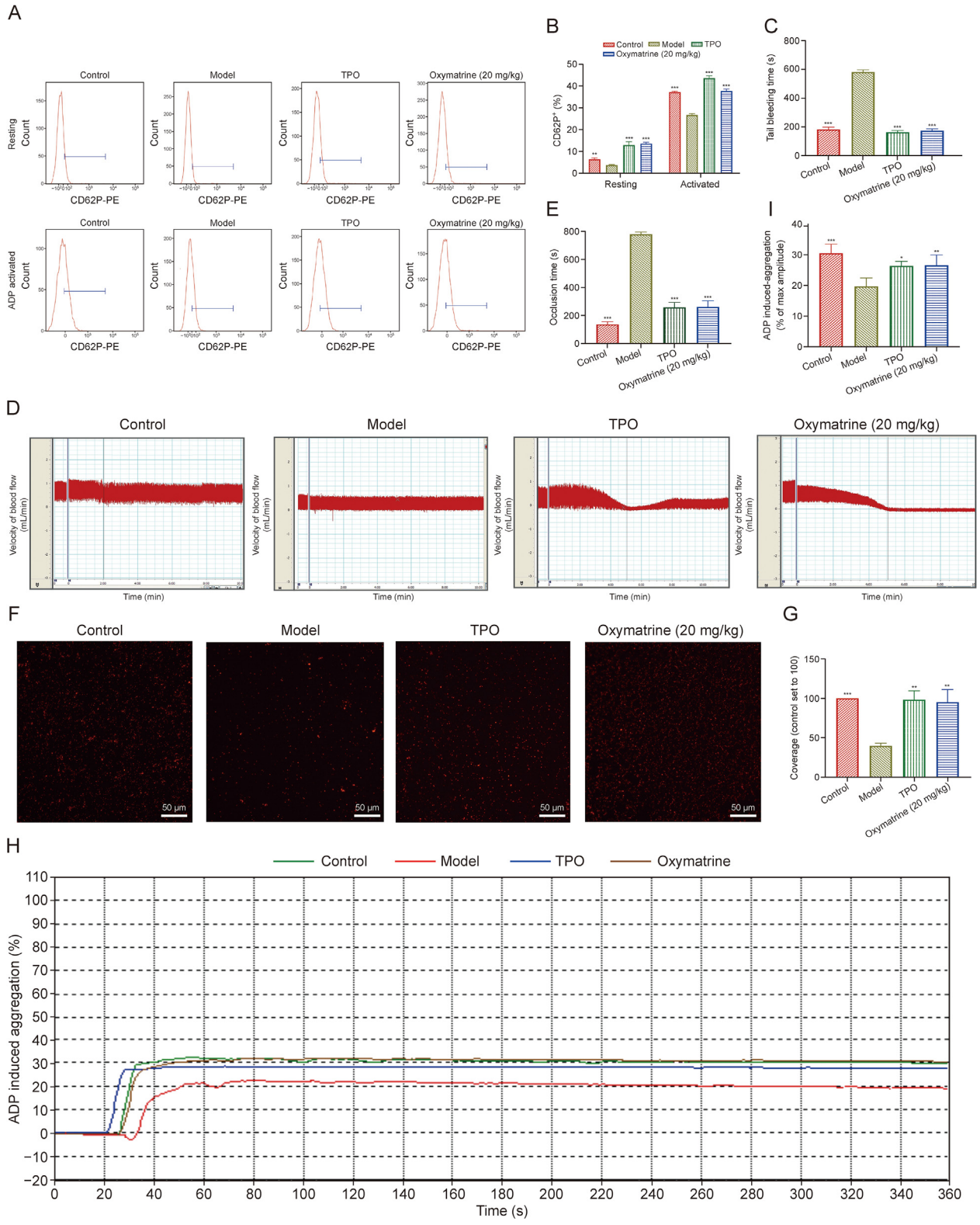

Fig. 6. Oxymatrine accelerates the recovery of platelet function in irradiated mice. (A) Flow cytometry analysis of $CD62P^+$ cells in washed platelets in control, model, thrombopoietin (TPO)-treated, and oxymatrine-treated groups (top), and the activated (adenosine diphosphate (ADP) 10 μM) $CD62P^+$ cells in each group (bottom). (B) The histogram shows the percentage of $CD62P^+$cells with or without ADP (10 μM) activation ($n = 3$ per group). (C) Tail bleeding time of each group after treatment of 12 days ($n = 3$ per group). (D) Analysis of carotid blood flow detection of each group. (E) The mean carotid artery occlusion times are represented by the histogram ($n = 3$ per group). (F) Micrographs of collagen-coated slides with the same number of platelets perfused. Red represents platelets. (G) The histogram shows the average coverage of red fluorescence on the whole surface by ImageJ software ($n = 3$ per group). (H) Platelet aggregation was detected under the activation of ADP by the device of turbidimetric aggregation-monitoring. (I) The histogram showed the maximum aggregation amplitude of platelets in each group ($n = 3$ per group). Data represent the mean ± standard deviation (SD) of three independent experiments. $^*P < 0.05$, $^{**}P < 0.01$, and $^{***}P < 0.001$ vs. the model group.

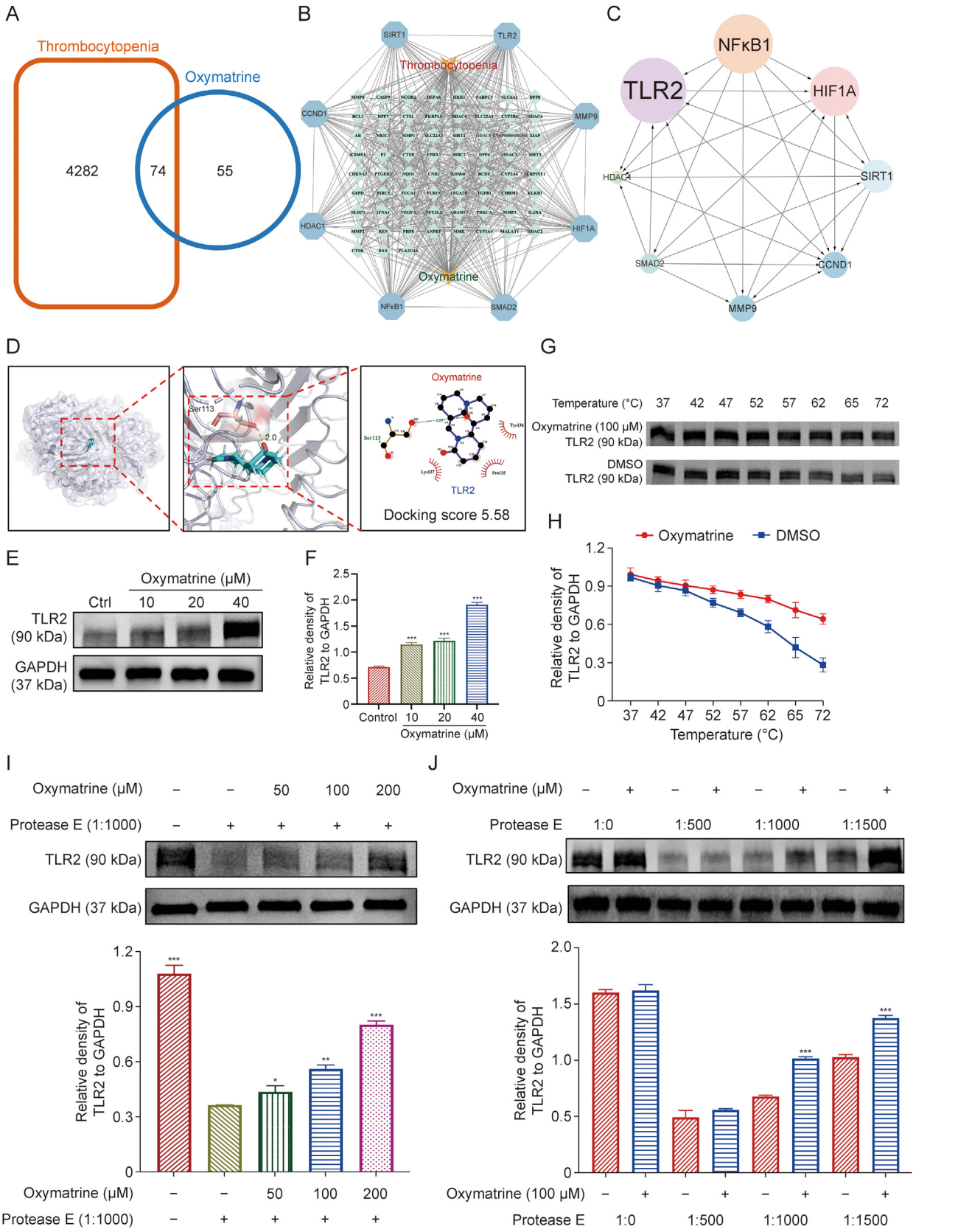

Fig. 7. Oxymatrine targets toll-like receptor 2 (TLR2) to induce magakaryocyte (MK) differentiation and thrombopoiesis. (A) Venn diagram exhibiting the shared targets of oxymatrine and thrombocytopenia. (B) The interaction of the shared targets analyzed by the Cytoscape_v3.7.1 software. (C) Protein-protein interaction (PPI) network for identifying the core target of oxymatrine against thrombocytopenia. (D) The molecular docking model for TLR2 and ligands (Oxymatrine). (E) After oxymatrine (10, 20, and 40 μM) intervened Meg-01 cells for five days, the representative immunoblot images and biochemical quantification of TLR2 were enhanced. (F) The histogram shows the relative density of TLR2 to glyceraldehyde-3-phosphate dehydrogenase (GAPDH) ($n = 3$ per group). (G) Cellular thermal shift assay (CETSA) analysis of TLR2 degradation damage under different temperatures.

consequent elevation of platelet levels in the treated group. This phenomenon can be attributed to the ability of oxymatrine to ameliorate hematopoietic progenitor cell function and stimulate progenitor cell differentiation toward the MK lineage.

3.6. Oxymatrine accelerates the recovery of platelet function in irradiated mice

Platelet activation plays an important role in hemostasis [53]. P-selectin (CD62P) is a glycoprotein that is present in the alpha granules of quiescent platelets and is known to be linked with their activation [54]. When platelets are activated, their shape dynamically changes, and they secrete alpha granules at the same time. The expression of CD62P can be used to estimate the level of cell degranulation and to monitor the state of platelet activation [55]. The response of platelets to physiological agonists can be used as an indicator of the availability of circulating platelets and depletion [54]. Therefore, we used flow cytometry to analyze CD62P expression in PB-washed platelets and found that the baseline level of CD62P in the TPO and oxymatrine-treated groups was higher than that in the model group. Furthermore, with ADP stimulation, the mice in the TPO and oxymatrine-treated groups were more sensitive to platelet reactivity (Figs. 6A and B). Meanwhile, the same activation was observed with collagen stimulation whereas the epinephrine was not (Fig. S3). These data indicated that oxymatrine-induced thrombopoiesis is functional. Moreover, tail bleeding time was measured to evaluate hemostatic function [56] and showed shorter tail bleeding times in the oxymatrine-treated (20 mg/kg) and TPO-treated groups than in the model group (Fig. 6C). An $FeCl_3$-induced carotid arterial thrombus model was established to evaluate the effect of oxymatrine on thrombogenesis (Fig. 6D). It is clear that the average occlusion times of the oxymatrine-treated (20 mg/kg) and TPO-treated groups were shorter than that of the model group (Fig. 6E), which indicates that oxymatrine possesses the ability to facilitate thrombus formation in irradiated mice. Similarly, after 12 days of treatment with oxymatrine and TPO, platelet adhesion was enhanced (Figs. 6F and G). Next, the platelet adhesion and aggregation induced by ADP on solidified collagen were measured (Fig. 6H), which showed that the percentage of ADP-induced platelet aggregation was markedly enhanced after treatment with oxymatrine and TPO for 12 days compared to the model group (Fig. 6I). Collectively, these findings illustrate that oxymatrine harbors promising therapeutic benefits for thrombocytopenia.

3.7. Oxymatrine targets TLR2 to induce MK differentiation and thrombopoiesis

To explore the potential therapeutic targets of oxymatrine for the management of thrombocytopenia, a network pharmacology approach was employed for target prediction. The molecular targets associated with oxymatrine were obtained from the SwissTargetPrediction database, whereas the molecular targets related to thrombocytopenia were obtained from the DisGeNET platform. We ultimately identified a total of 74 potential targets for the oxymatrine-mediated treatment of thrombocytopenia (Fig. 7A). The present study involved the importation of the desired targets into Cytoscape_v3.7.1, a bioinformatics tool that enables the generation of an interaction network. The obtained PPI results demonstrated that TLR2 may function as a core target (Figs. 7B and C). Subsequently, a molecular docking model was used to assess the potential of oxymatrine for TLR2 binding. The results exhibited that oxymatrine formed hydrogen bonds with SER-116 amino acid residues on TLR2 protein. A docking score exceeding 5 kcal/mol is commonly regarded as an indicator of substantial binding affinity. The findings of the study revealed a docking score of 5.58 for the binding of oxymatrine to TLR2, which suggested the substantial affinity of oxymatrine for this receptor (Fig. 7D). Moreover, we found that the expression of TLR2 was upregulated in a concentration-dependent manner after oxymatrine intervention in Meg-01 cells for five days (Figs. 7E and F). Furthermore, in order to further elucidate the interaction between oxymatrine and TLR2, CETSA assay was performed. As exhibited in Figs. 7G and H, the treatment of oxymatrine to heat-denatured Meg-01 cells lysayes led to the stabilization of TLR2 as various temperatures. To further demonstrate the targeting of oxymatrine to TLR2, a DARTS assay was conducted. According to the data obtained from DARTS analysis, oxymatrine protects against protease-induced degradation of TLR2. This outcome is in accordance with the high affinity of oxymatrine for TLR2. (Figs. 7I and J). Taken together, these findings suggest that TLR2 represents a potential molecular target mediating the promotion of megakaryocytic differentiation and thrombopoiesis by oxymatrine.

3.8. Oxymatrine induces MKs differentiation by regulating the STING/NF-κB pathway

To establish the fundamental mechanism underlying the stimulatory effects of oxymatrine on the differentiation of MKs, network pharmacology was applied. KEGG pathway analysis identified the 20 pathways most likely involved in the oxymatrine-mediated differentiation of MK cells. The enrichment analyses revealed a conspicuous prevalence of genes within the TLR signaling and NF-κB signaling pathways, which are known to play crucial roles in the processes of MK differentiation and platelet function (Fig. 8A). Oxymatrine targets TLR2, which plays an important role in promoting MK differentiation. Moreover, evidence has been shown that activated TLR2 can induce the STING/NF-κB cascade. Therefore, we speculate that STING/IκBα/NF-κB is involved in oxymatrine-induced MK differentiation. The data obtained from the WB assay revealed a concentration-dependent increase in the expression levels of extracellular regulated kinase 1/2 (ERK1/2), phosphorylated STING, phosphorylated IκBα, and phosphorylated NF-κB in the group treated with oxymatrine compared to those in the control group (Figs. 8B–E). Subsequently, several TFs were analyzed, and the results indicated that the expression of RUNX1, NF-E2, EGR1, and FOS was strongly upregulated by oxymatrine, which is vital for MK differentiation (Figs. 8F–I). Furthermore, we performed immunofluorescence staining for TLR2/p-STING/p-NF-κB on BM sections from oxy-treated thrombocytopenia mouse. The results showed that expression of TLR2/p-STING/p-NF-κB in the oxymatrine group could be expressed on the same cells, while the fluorescence expression of those was higher than that in the model group (Fig. 8J). Moreover, the expression NF-E2 and RUNX1, transcriptional regulators with therapeutic significance, was upregulated in Meg-01 cells following treatment with oxymatrine (Figs. 8K and L) and in K-562 cells (Fig. S4). In addition, the TLR2-specific inhibitor C29 and the STING-specific inhibitor C-176 were loaded. After Meg-01 cells were treated

(H) The histogram shows the relative density of TLR2 to GAPDH ($n = 3$ per group). (I) The drug affinity responsive target stability assay (DARTS) assay indicated oxymatrine blinding to the TLR2 in a concentration-dependent manner. Treatment with protease (1:1000) was conducted for 10 min at 40 °C ($n = 3$ per group). (J) DARTS assay for target validation. The stability of protein TLR2 was enhanced upon the treatment of oxymatrine (100 μM) in Meg-01 lysates. Concentration gradient (1:500, 1:1000, and 1:1500) protease was added for 60 μg/mL stock for 10 min at 40 °C ($n = 3$ per group). Data represent the mean ± standard deviation (SD) of three independent experiments. $^{*}P < 0.05$, $^{**}P < 0.01$, and $^{***}P < 0.001$ vs. the control group. NFκB1: nuclear factor kappaB subunit 1; DMSO: dimethyl sulfoxide.

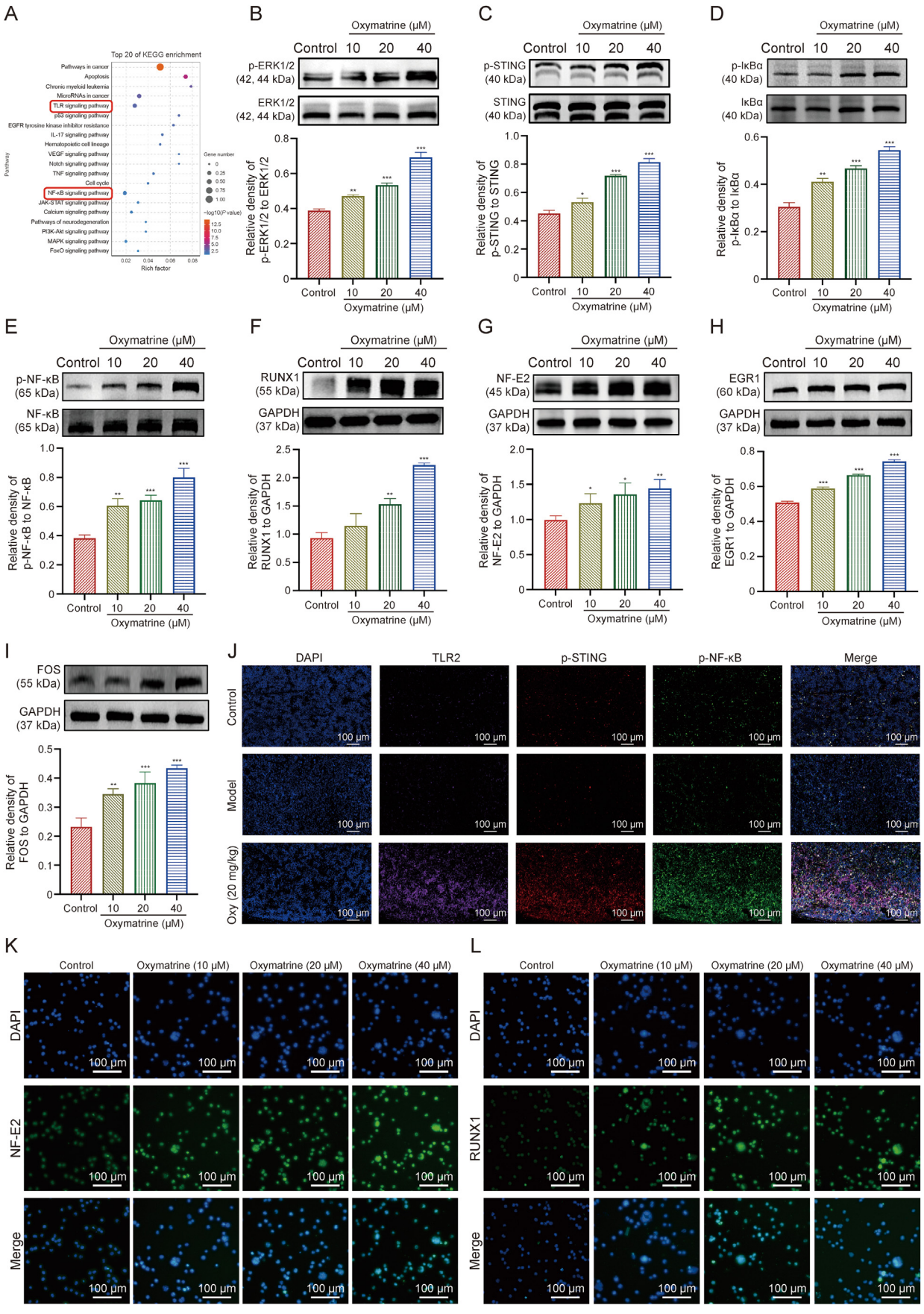
A
Top 20 of KEGG enrichment
Pathways in cancer
Apoptosis
Chronic myeloid leukemia
MicroRNAs in cancer
TLR signaling pathway
p53 signaling pathway
EGFR tyrosine kinase inhibitor resistance
IL-17 signaling pathway
Hematopoietic cell lineage
VEGF signaling pathway
Notch signaling pathway
TNF signaling pathway
Cell cycle
NF-κB signaling pathway
JAK-STAT signaling pathway
Calcium signaling pathway
Pathways of neurodegeneration
PI3K-Akt signaling pathway
MAPK signaling pathway
FoxO signaling pathway
Pathway
Rich factor
Gene number
-log10(P.value)
B
Oxymatrine (μM)
Control 10 20 40
p-ERK1/2 (42, 44 kDa)
ERK1/2 (42, 44 kDa)
Relative density of p-ERK1/2 to ERK1/2
C
p-STING (40 kDa)
STING (40 kDa)
Relative density of p-STING to STING
D
p-IκBα (40 kDa)
IκBα (40 kDa)
Relative density of p-IκBα to IκBα
E
p-NF-κB (65 kDa)
NF-κB (65 kDa)
Relative density of p-NF-κB to NF-κB
F
RUNX1 (55 kDa)
GAPDH (37 kDa)
Relative density of RUNX1 to GAPDH
G
NF-E2 (45 kDa)
GAPDH (37 kDa)
Relative density of NF-E2 to GAPDH
H
EGR1 (60 kDa)
GAPDH (37 kDa)
Relative density of EGR1 to GAPDH
I
FOS (55 kDa)
GAPDH (37 kDa)
Relative density of FOS to GAPDH
J
DAPI
TLR2
p-STING
p-NF-κB
Merge
Control
Model
Oxy (20 mg/kg)
100 μm
K
Control
Oxymatrine (10 μM)
Oxymatrine (20 μM)
Oxymatrine (40 μM)
DAPI
NF-E2
Merge
L
RUNX1

for five days, the number of MKs with large cell sizes decreased after oxymatrine was loaded with C29 and C-176 (Figs. 9A and B). Moreover, the fluorescence intensity of F-actin aggregates (phalloidin staining) was attenuated after oxymatrine was loaded with C29 and C-176 (Figs. 9C and D). The cell surface markers CD41 and CD42b are considered as indicators of MK differentiation. We analyzed the percentage of $CD41^{+}/CD42b^{+}$ cells with or without C29 or C-176 treatment and discovered that C29 and C-176 significantly inhibited the induction of MK differentiation induced by oxymatrine, in comparison to that in the group of Meg-01 cells treated with oxymatrine (Figs. 9E and F). The findings of this study suggest that C29 can obstruct the expression of TLR2 using Pam3CSK4 as positive control (Fig. S5), in addition to causing a notable reduction in the levels of p-STING and p-NF-κB within the group treated with oxymatrine, as shown by the WB assay data (Figs. 9G–J). The STING inhibitor, C-176, was found to downregulate the levels of p-STING and p-NF-κB, without affecting the expression of TLR2 (Figs. 9K–N). Taken together, the findings of this study imply that oxymatrine tends to act on the STING/NF-κB signaling pathway subsequent to TLR2 activation, thus leading to the initiation of megakaryocytic differentiation as well as the formation and functionalization of platelets. These results are indicative of the therapeutic potential of oxymatrine for treating platelet-related ailments.

4. Discussion

Thrombocytopenia, a severe complication of radiation therapy, remains an obstacle to treatment and reduces the overall survival rate of patients [57]. The foremost coordinate hematologic definition of thrombocytopenia could be a decrease within the number of PB plates. Platelets plays a critical role in primary hemostasis and be incolved in multiple nonhemostatic biological process such as angiogenesis, tissue repair, inflammation, and metastatis [58]. Hence, once the counts of platelet diminishes, the patients with hematologic clutters and thrombocytopenia have an expanded chance of bleeding. Although there are several treatment options, such as platelet transfusion and platelet damage reduction, serious adverse reactions can occur [59,60]. Thus, stimulating the production of platelets appears to be a feasible strategy for thrombocytopenia therapy. TPO-RAs are widely reported to regulate megakaryopoiesis and thrombopoiesis [10]. To date, three oral nonpeptide TPO-RAs have been used in the clinic [61]. Nevertheless, patients with TPO-RA resistance or mutations in the *c-MPL* (thrombopoietin receptor protein) gene are unlikely to benefit from the present therapy [62,63]. Therefore, small-molecule compounds that are independent of the TPO-cMPL pathway are urgently needed for the treatment of thrombocytopenia.

Oxymatrine is extracted from the roots of Sophora flavescens Ait, which possess admirable pharmacological effects, including antiviral and other immune-regulating effects [32,33]. However, the pharmacological effects in promoting megakaryopoiesis and thrombopoiesis has not been reported yet. Hence, we firstly demonstrated the potential effect of promoting MKs differentiation and PPF *in vitro* with two MK cell lines, K-562 and Meg-01 [64]. The results exhibited that oxymatrine promoted MKs differentiation with concentration depend manner (Figs. 1E and 2). Meanwhile, to confirm that the concentration extend of the sedate we chosen was not poisonous to MKs, we analyzed the LDH of MKs after treatment of oxymatrine. It was found that oxymatrine was non toxic to MKs (Figs. 1A–D). Apoptosis is considered as a crucial biological process in thrombopoiesis [47]. The current research investigated that both K-562 and Meg-01 cell treated with oxymatrine for five days exhibited early apoptosis (Fig. S1). Combined with the results of LDH analysis, it might be the proliferation inhibition effect of oxymatrine, which lead to the number of MK less than the control and ultimately result in the no difference of LDH between control and oxymatrine treated group. Meanwhile, in apoptosis, the cells shrink with integral but ruffling plasma membranes, and chromatin is condensed and fragmented. The cells don't spill their contents into the surrounding environment. Cells undergoing necrosis swell and lose membrane integrity, which is followed by spillage of the intracellular contents including LDH into surrounding areas [65–67]. Once cells are impaired by traumatic events, toxic chemicals, stress, or intercellular signals, plasma membrane will disrupt and LDH will be rapidly released into the surrounding extracellular space. Therefore, the results of LDH assay cannot completely represent cellular apoptosis. Therefore, the effect of oxymatrine on MK apoptosis is worthy of further investigation. The obove all results exhibited oxymatrine possessed the potential to stimulate the differentiation of MKs and facilitate the production of platelets.

However, the two human MK model cell lines, K-562 and Meg-01 rather than primary cells, we used for verification of the degree of MKs differentiation still faces certain limitations [68,69]. Hence, the model of zebrafish was involved. Notably, the zebrafish model has been widely used in multiple fields, such as drug discovery, toxicology, and developmental biology, and is a prominent vertebrate model that possesses the advantages of *in vitro* screening convenience and *in vivo* complexity compared with the normal mouse model. Hence, Tg (cd41:eGFP) zebrafish were utilized, and we observed that oxymatrine significantly expanded hematopoietic stem and progenitor cells (HSPCs) and thrombocytes by analyzing the ratio of $CD41{:}GFP^{+}$ cells in zebrafish embryos (Fig. 3). Furthermore, the effects of oxymatrine on thrombopoiesis were verified in the RIT mouse model. Prior to the formal experiments, extensive preliminary investigations were conducted to determine the optimal dosing regimen for oxymatrine. These experiments involved administering various concentrations of oxymatrine to RIT mice. Based on the results, a single dose of 20 mg/kg oxymatrine administered through intraperitoneal injection exhibited the greatest therapeutic efficacy in RIT mice. Consequently, this dose was chosen for the subsequent formal experiments. After the administration of oxymatrine for 12 days, we found that oxymatrine (20 mg/kg) significantly increased

Fig. 8. Oxymatrine induces megakaryocyte (MK) differentiation by activating stimulator of interferon genes (STING)/nuclear factor-kappaB (NF-κB) pathway. (A) Kyoto Encyclopedia of Genes and Genomes (KEGG) pathway enrichment analysis for the potential pathway by which oxymatrine promotes MK differentiation. (B–E) Western blot (WB) analysis of the expression of pathway: extracellular regulated kinase 1/2 (ERK1/2)/STING/inhibitory subunit of nuclear factor kappa B alpha (IκBα)/NF-κB by which oxymatrine promotes MK differentiation. Representative immunoblot images and biochemical quantification of the ERK1/2 (B), STING (C), IκBα (D), and NF-κB (E) pathway after the treatment with oxymatrine (10, 20, and 40 μM) in Meg-01 cells for five days ($n = 3$ per group). (F–I) Representative immunoblot images and biochemical quantification of the transcription factors (TFs) associated with MK differentiation: runt-related transcription factor 1 (RUNX1) (F), nuclear factor erythroid 2 (NF-E2) (G), early growth response protein 1 (EGR1) (H), and cellular oncogene fos (FOS) (I) ($n = 3$ per group). (J) Representative immunofluorescence images of toll-like receptor 2 (TLR2) fluorescently triple-stained with p-STING and p-NF-κB, respectively, on bone marrow (BM) cells after 12 days of treatment with oxymatrine in a mouse model of radiation thrombocytopenia. Blue for the 4′,6-diamidino-2-phenylindole (DAPI), purple for the TLR2, red for the p-STING, and green for the p-NF-κB. (K, L) Representative images of immunofluorescence of the nuclear translocation of NF-E2 (K) and RUNX1 (L) in Meg-01 cells after the treatment of oxymatrine for five days. Excitation wavelengths: 470 nm for NF-E2 and RUNX1 and 405 nm for DAPI. Data represent the mean ± standard deviation (SD) of three independent experiments. $^{*}P < 0.05$, $^{**}P < 0.01$, and $^{***}P < 0.001$ vs. the control group. EGFR: epidermal growth factor receptor; IL-17: interleukin 17; VEGF: vascular endothelial growth factor ; TNF: tumor necrosis factor; JAK-STAT: janus kinase-signal transducer and activator of transcription; PI3K-Akt: phospholnositide-3 kinase-threonine kinase B; MAPK: mitogen-activated protein kinase; FoxO: forkhead box protein O; GAPDH: glyceraldehyde-3-phosphate dehydrogenase.

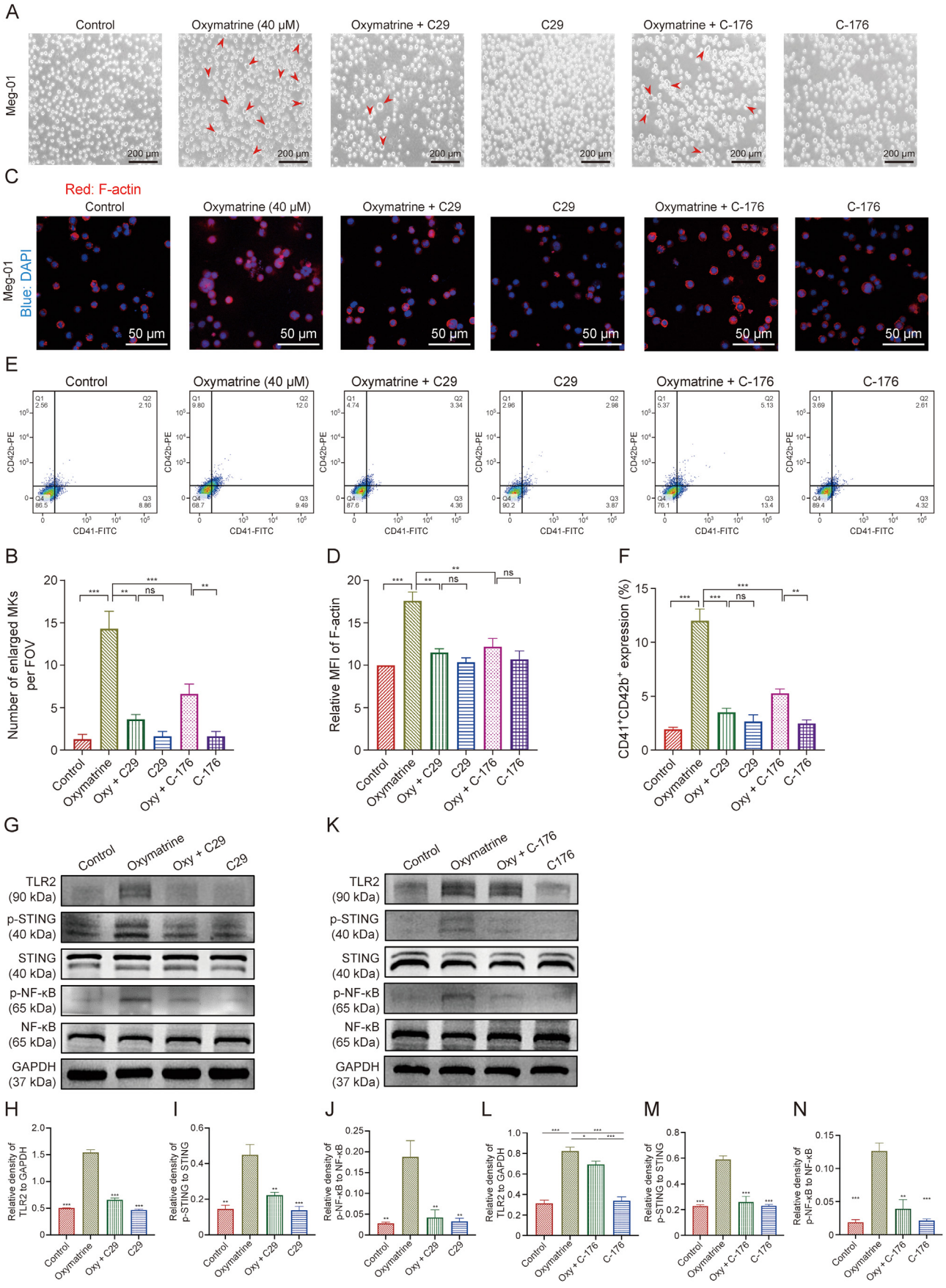
A
Control
Oxymatrine (40 μM)
Oxymatrine + C29
C29
Oxymatrine + C-176
C-176
Meg-01
200 μm
C
Red: F-actin
Blue: DAPI
50 μm
E
CD42b-PE
CD41-FITC
B
Number of enlarged MKs per FOV
D
Relative MFI of F-actin
F
CD41+CD42b+ expression (%)
G
K
TLR2 (90 kDa)
p-STING (40 kDa)
STING (40 kDa)
p-NF-κB (65 kDa)
NF-κB (65 kDa)
GAPDH (37 kDa)
H
Relative density of TLR2 to GAPDH
I
Relative density of p-STING to STING
J
Relative density of p-NF-κB to NF-κB
L
M
N

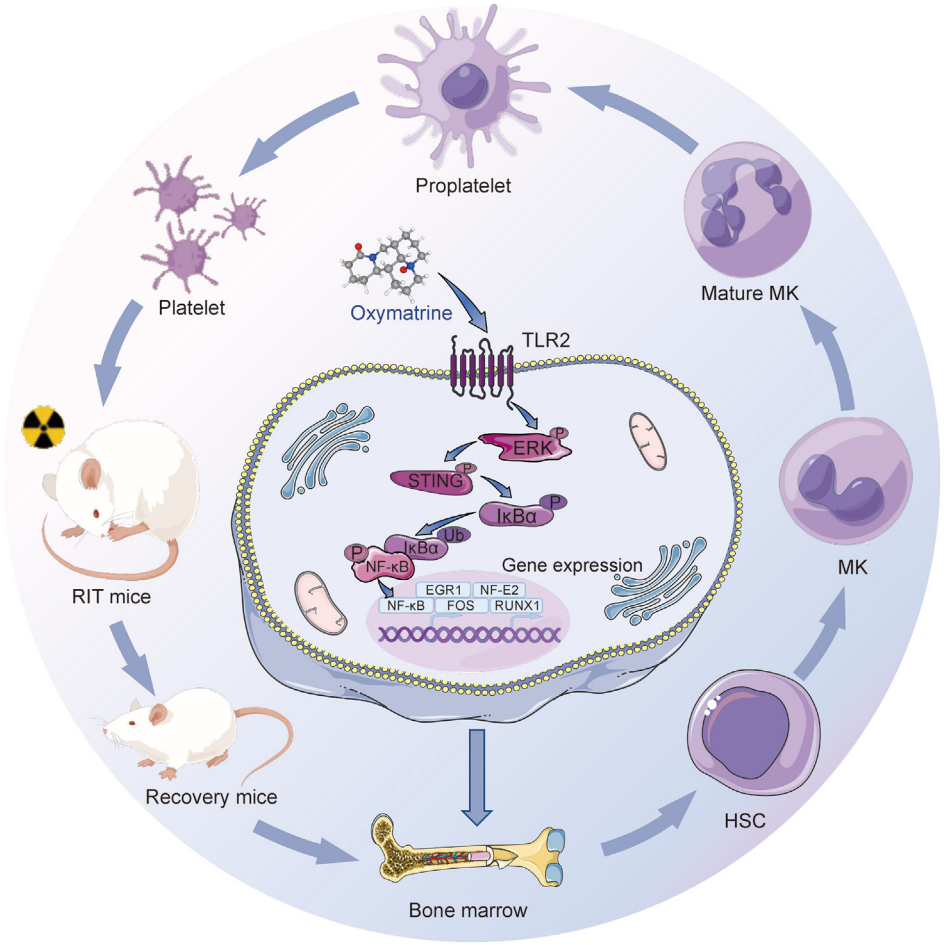

Fig. 10. The schematic illustration of oxymatrine regulating megakaryocyte (MK) differentiation and thrombopoiesis. Oxymatrine targets toll-like receptor 2 (TLR2) and activates the downstream extracellular regulated kinase 1/2 (ERK1/2)/stimulator of interferon genes (STING)/inhibitory subunit of nuclear factor kappa B alpha (IκBα)/nuclear factor-kappaB (NF-κB) signaling pathway, which leads to the high expression of transcription factors (TFs): early growth response 1 (EGR1), nuclear factor erythroid 2 (NF-E2), cellular oncogene fos (FOS), and runt-related transcription factor 1 (RUNX1). As a result, the activated transcription factors promote the expression of megakaryopoiesis and thrombopoiesis related genes, which contribute to the MK maturation and platelet production and finally recover the platelet levels in adiation-induced thrombocytopenia mice. RIT: radiation-induced thrombocytopenia; HSC: hematopoietic stem cell; ERK: extracellular regulated kinase; Ub: ubiquitin.

peripheral platelet levels and accelerated the platelet recovery time (Figs. 4B–F). These data further demonstrated that oxymatrine possess admirable potential therapeutic effects for thrombocytopenia. In consideration of our mice model was established by radiation and the BM is quiet sensitive to the radiation damage [70]. The H&E and flow cytometry were firstly perfomed to examined the morphological and overall counts changes in BM and spleen. The results of BM H&E staining and flow cytometry demonstrated that oxymatrine promoted megakaryopoiesis by stimulating the differentiation of hematopoietic progenitor cells (Figs. 5A and E). Moreover, the analysis of spleen H&E staining and flow cytometry revealed that oxymatrine treatment elevated the splenic MK count, where EMH was enhanced (Figs. 5C and G). Subsequently, due to the thrombocytopenic mice encounter platelet dysfunction, which was caused by the low platelet count and platelet damage, the risks of bleeding is potentially increased. Therefore, to detect platelet function recovery after oxymatrine treatment, we perfomed a series of platelet function testing analyses. A $FeCl_3$ induced carotid arterial thrombus model was used, and platelet adhesion and aggregation assays were performed. The results demonstrated that oxymatrine could restore the function of platelets and possess a beneficial effect on hemostasis under pathological conditions (Fig. 6). Taken together, all these data suggest that the effect of oxymatrine on hematopoiesis is multifaceted and multisite, which makes oxymatrine as a potential candidate to mitigate RIT.

Fig. 9. The effect of megakaryocyte (MK) differentiation induced by oxymatrine was block by toll-like receptor 2 (TLR2) inhibitor C29 and stimulator of interferon genes (STING) inhibitor C-176. (A) Representative images of oxymatrine treated Meg-01 cells with oxymatrine (40 μM), C29 (50 μM), oxymatrine (40 μM) + C29 (50 μM), C-176 (10 μM), and oxymatrine (40 μM) + C-176 (10 μM) for five days. (B) The histogram represents the number of MKs in each group ($n = 3$ per group). (C) Phalloidin-labeled cytospin in Meg-01 cells intervened with oxymatrine (40 μM), C29 (50 μM), oxymatrine (40 μM) + C29 (50 μM), C-176 (10 μM), and oxymatrine (40 μM) + C-176 (10 μM) for five days under a fluorescence Microscope. Excitation wavelength: 560 nm for phalloidin and 405 nm for 4′,6-diamidino-2-phenylindole (DAPI). (D) The histogram represents the relative mean fluorescence intensity (MFI) of F-actin in each group ($n = 3$ per group). (E) Flow cytometry analysis exhibits the percentage of $CD41^+/CD42^+$ cells after the treatment of oxymatrine (40 μM), C29 (50 μM), oxymatrine (40 μM) + C29 (50 μM), C-176 (10 μM), and oxymatrine (40 μM) + C-176 (10 μM) for five days. (F) The histogram represents the percentage of $CD41^+/CD42b^+$ expression in each group ($n = 3$ per group). (G–J) Representative immunoblot images (G) and biochemical quantification of TLR2 (H), STING (I), and nuclear factor-kappaB (NF-κB) (J) after the treatment of oxymatrine (40 μM), C29 (50 μM), and oxymatrine (40 μM) + C29 (50 μM) for five days ($n = 3$ per group). (K–N) Representative immunoblot images (K) and biochemical quantification of TLR2 (L), STING (M), and NF-κB (N) after the treatment of oxymatrine (40 μM), C-176 (10 μM), and oxymatrine (40 μM) + C-176 (10 μM) for five days ($n = 3$ per group). Data represent the mean ± standard deviation (SD) of three independent experiments. $^*P < 0.05$, $^{**}P < 0.01$, and $^{***}P < 0.001$ vs. the oxymatrine group. ns: no significance. PE: phycoerythrin; FITC: fluorescein isothiocyanate; FOV: field of view; GAPDH: glyceraldehyde-3-phosphate dehydrogenase.

TLR2 and TLR4 are the main receptors in the TLRs family and are related to thrombopoiesis and platelet activation [71,72]. Reports have demonstrated that TLRs are expressed in MKs. The activation of TLRs affects three main aspects of platelets: the regulation of platelet biogenesis and the regulation of proinflammatory and antiviral responses [25,73]. TLR2 mediates intracellular activation through the myeloid differentiation primary response 88 (MyD88)-dependent pathway [74], which can activate downstream pathways, including the MAPK and NF-κB pathways [75]. Previous studies have demonstrated that NF-κB inhibition can interfere with platelet function by reducing its thrombogenic potential [76]. Interestingly, emerging research corroborates that NF-κB plays a role in positively regulating platelet survival, priming, activation, and aggregation [77,78]. STING is an ER junction and sensing protein that can interact with the immune response and participate in multiple regulatory processes, such as cancer and inflammation [79,80]. Recent reports have demonstrated that the STING pathway is associated with platelet activation and granule secretion [24]. Moreover, the role of STING activation in TLR2/NF-κB has signaling been reported [29]. However, how STING interacts with MK differentiation and thrombopoiesis is a perplexing and equally interesting issue. Similarly, in our present research, network pharmacological prediction analysis revealed that TLR2 was a potential target of oxymatrine for the treatment of thrombocytopenia (Figs. 7A–C). Moreover, the interaction between oxymatrine and TLR2 was imitated by molecular docking, which showed that the total docking score was 5.58, indicating stable binding (Fig. 7D). In addition, CETSA and DRATS assay was performed, which demonstrated that oxymatrine markedly increased the stability of TLR2 by directly binding to it (Figs. 7G–J). Therefore, we speculate that the binding of genistin to TLR2 may trigger downstream signaling pathways that promote MK differentiation and platelet formation. By using the network pharmacology pathway enrichment, we discovered the TLRs pathway and NF-κB pathway was significantly enriched. We examined the effect of oxymatrine on the protein expression of STING/NF-κB signaling pathways and the MKs differentiation related key TFs and found that it showed an upregulated trend (Figs. 8A–I and K). Meanwhile, we further investigated the expression of TLR2/p-STING/p-NF-κB in the BM of RIT mice treated with oxymatrine and found that they were all upregulated (Fig. 8J). Furthermore, by loading specific inhibitors of TLR2 and STING, C29 or C-176 blocked the effect of oxymatrine on MK differentiation (Fig. 9). Ultimately, we identified oxymatrine by binding to the primary receptor TLR2, triggering downstream STING/NF-κB activation and promoting MK differentiation and thrombopoiesis (Fig. 10).

Although studies have reported that oxymatrine can inhibit TLRs and downstream NF-κB [32,81], we demonstrated that oxymatrine targets TLR2 and activates the STING/NF-κB pathway to induce MK differentiation and platelet formation. This phenomenon has been demonstrated in different biological models, and the regulatory mechanism of drugs can vary. TLR2, as a pattern recognition receptor, is associated with multiple signaling pathways; however, its interaction with STING has rarely been reported. In our research, we found that oxymatrine (10, 20, and 40 μM) can significantly induce the differentiation of K-562 and Meg-01 MKs. In addition, an intraperitoneal injection of 20 mg/kg oxymatrine intraperitoneally promoted platelet recovery in RIT model mice. However, the *in vitro* experiments still require extensive biological replication to determine whether the activation of the TLR2/STING/NF-κB axis can influence the release of inflammatory factors and whether proof for direct drug-target binding (surface plasmon resonance) is important. For further investigation of the oxymatrine-mediated promotion of MK differentiation, vital cellular models (human $CD34^+$ hematopoietic progenitor cells) need to be developed. Taken together, our research demonstrated that oxymatrine, a novel TLR2 agonist, potentially promotes megakaryopoiesis and thrombopoiesis via the TLR2/STING/NF-κB axis.

5. Conclusion

In the present study, the potential and intricate molecular mechanism through which oxymatrine stimulates megakaryopoiesis and facilitates recovery following radiation-induced RIT were elucidated for the first time. The present research revealed the promotive effect of oxymatrine on MK differentiation *in vitro*, while simultaneously demonstrating its potential to restore platelet count and promote functional recovery in mice experiencing RIT. Additionally, our findings demonstrated the capacity of oxymatrine to bind to TLR2, thereby initiating STING/NF-κB cascade signaling and promoting the differentiation of MKs. In brief, the evidence presented in this study yields favorable data regarding the mode of action of oxymatrine in the context of RIT therapy. Moreover, these findings suggest that oxymatrine is a potential therapeutic agent and holds promise as a drug in RIT therapy.

CRediT authorship contribution statement

Chengyang Ni: Writing – original draft, Investigation, Conceptualization. **Ling Zhou:** Resources, Methodology, Investigation. **Shuo Yang:** Validation, Supervision, Methodology. **Mei Ran:** Validation, Resources, Methodology. **Jiesi Luo:** Software, Resources, Investigation. **Kui Cheng:** Supervision, Resources, Methodology. **Feihong Huang:** Supervision, Software, Methodology. **Xiaoqin Tang:** Validation, Methodology, Investigation. **Xiang Xie:** Validation, Supervision, Resources. **Dalian Qin:** Supervision, Resources. **Qibing Mei:** Supervision, Resources, Methodology. **Long Wang:** Writing – review & editing, Supervision, Formal analysis. **Juan Xiao:** Writing – review & editing, Validation, Supervision. **Jianming Wu:** Writing – review & editing, Supervision, Funding acquisition, Conceptualization.

Declaration of competing interest

The authors declare that there are no conflicts of interest.

Acknowledgments

The present study was supported by grants from the National Natural Science Foundation of China (Grant Nos.: 82074129, 82004073, 82204666, and 82374073); the Science and Technology Planning Project of Sichuan Province, China (Grant Nos.: 2022JDJQ0061, 2022ZYD0087, 2022YFS0607, 2022YFS0635, and 2022YFS0635-B1); the Joint Project of Xuzhou District People's Government and Southwest Medical University, China (Grant No.: 2021XZXNYD01), and Science and Technology Planning Project of Yibin City, China (Grant Nos.: 2022NY020, 2021ZYY009, and 2021ZYY005). We express our thanks to Figdraw for providing the figure icons.

Appendix A. Supplementary data

Supplementary data to this article can be found online at https://doi.org/10.1016/j.jpha.2024.101054.

References

[1] C. Ni, Y. Wu, M. Ran, et al., Design, synthesis and evaluation of novel dehydroabietic acid-dithiocarbamate hybrids as potential multi-targeted compounds for tumor cytotoxicity, Arab. J. Chem. 15 (2022), 104145.

[2] J. Ferlay, M. Colombet, I. Soerjomataram, et al., Estimating the global cancer incidence and mortality in 2018: GLOBOCAN sources and methods, Int. J. Cancer 144 (2019) 1941–1953.
[3] W. Hur, S.K. Yoon, Molecular pathogenesis of radiation-induced cell toxicity in stem cells, Int. J. Mol. Sci. 18 (2017), 2749.
[4] D.I. Bunin, J. Bakke, C.E. Green, et al., Romiplostim (Nplate®) as an effective radiation countermeasure to improve survival and platelet recovery in mice, Int. J. Radiat. Biol. 96 (2020) 145–154.
[5] E. Tkaczynski, A. Arulselvan, J. Tkaczynski, et al., 2-*O*, 3-*O* desulfated heparin mitigates murine chemotherapy- and radiation-induced thrombocytopenia, Blood Adv. 2 (2018) 754–761.
[6] K. Eto, S. Kunishima, Linkage between the mechanisms of thrombocytopenia and thrombopoiesis, Blood 127 (2016) 1234–1241.
[7] J.N. George, Platelets, Lancet 355 (2000) 1531–1539.
[8] F. Che, J. Zhao, Y. Zhao, et al., A novel heterozygous pathogenic variation in *CYCS* gene cause autosomal dominant non-syndromic thrombocytopenia 4 in a large Chinese family, Front. Genet. 12 (2022), 783455.
[9] M.P. Busch, E.M. Bloch, S. Kleinman, Prevention of transfusion-transmitted infections, Blood 133 (2019) 1854–1864.
[10] W. Ghanima, N. Cooper, F. Rodeghiero, et al., Thrombopoietin receptor agonists: Ten years later, Haematologica 104 (2019) 1112–1123.
[11] A. Constantinescu-Bercu, Y.A. Wang, K.J. Woollard, et al., The GPIbα intracellular tail - role in transducing VWF- and collagen/GPVI-mediated signaling, Haematologica 107 (2022) 933–946.
[12] Q. Wang, J. Li, T. Yu, et al., Disrupted balance of $CD4^+$ T-cell subsets in bone marrow of patients with primary immune thrombocytopenia, Int. J. Biol. Sci. 15 (2019) 2798–2814.
[13] S. Dütting, F. Gaits-Iacovoni, D. Stegner, et al., A Cdc42/RhoA regulatory circuit downstream of glycoprotein Ib guides transendothelial platelet biogenesis, Nat. Commun. 8 (2017), 15838.
[14] S. Borst, X. Sim, M. Poncz, et al., Induced pluripotent stem cell-derived megakaryocytes and platelets for disease modeling and future clinical applications, Arterioscler. Thromb. Vasc. Biol. 37 (2017) 2007–2013.
[15] E. Bianchi, R. Norfo, V. Pennucci, et al., Genomic landscape of megakaryopoiesis and platelet function defects, Blood 127 (2016) 1249–1259.
[16] J. Pan, L. Lordier, D. Meyran, et al., The formin DIAPH1 (mDia1) regulates megakaryocyte proplatelet formation by remodeling the actin and microtubule cytoskeletons, Blood 124 (2014) 3967–3977.
[17] J. Lin, J. Zeng, S. Liu, et al., DMAG, a novel countermeasure for the treatment of thrombocytopenia, Mol. Med. 27 (2021), 149.
[18] Y. Qing, X. Wang, H. Wang, et al., Pharmacologic targeting of the P-TEFb complex as a therapeutic strategy for chronic myeloid leukemia, Cell Commun. Signal. 19 (2021), 83.
[19] P.J. Kranzusch, S.C. Wilson, A.S.Y. Lee, et al., Ancient origin of cGAS-STING reveals mechanism of universal 2',3' cGAMP signaling, Mol. Cell 59 (2015) 891–903.
[20] X. Tan, L. Sun, J. Chen, et al., Detection of microbial infections through innate immune sensing of nucleic acids, Annu. Rev. Microbiol. 72 (2018) 447–478.
[21] Q. Chen, L. Sun, Z.J. Chen, Regulation and function of the cGAS-STING pathway of cytosolic DNA sensing, Nat. Immunol. 17 (2016) 1142–1149.
[22] M. Jiang, P. Chen, L. Wang, et al., cGAS-STING, an important pathway in cancer immunotherapy, J. Hematol. Oncol. 13 (2020), 81.
[23] J. Kwon, S.F. Bakhoum, The cytosolic DNA-sensing cGAS-STING pathway in cancer, Cancer Discov. 10 (2020) 26–39.
[24] M. Yang, H. Jiang, C. Ding, et al., STING activation in platelets aggravates septic thrombosis by enhancing platelet activation and granule secretion, Immunity 56 (2023) 1013–1026.e6.
[25] X. Tang, Q. Xu, S. Yang, et al., Toll-like receptors and thrombopoiesis, Int. J. Mol. Sci. 24 (2023), 1010.
[26] L.M. Beaulieu, E. Lin, K.M. Morin, et al., Regulatory effects of TLR2 on megakaryocytic cell function, Blood 117 (2011) 5963–5974.
[27] N. Kovuru, S. Raghuwanshi, A. Sangeeth, et al., Co-stimulatory effect of TLR2 and TLR4 stimulation on megakaryocytic development is mediated through PI3K/NF-κB and XBP-1 loop, Cell. Signal. 80 (2021), 109924.
[28] J. Zeng, W. Sun, J. Chang, et al., *HOXC4* up-regulates NF-κB signaling and promotes the cell proliferation to drive development of human hematopoiesis, especially $CD43^+$ cells, Blood Sci. 2 (2020) 117–128.
[29] C.C.B. Bomfim, L. Fisher, E.P. Amaral, et al., *Mycobacterium tuberculosis* induces Irg1 in murine macrophages by a pathway involving both TLR-2 and STING/IFNAR signaling and requiring bacterial phagocytosis, Front. Cell. Infect. Microbiol. 12 (2022), 862582.
[30] K. Grundler, R. Rotter, S. Tilley, et al., The proteasome regulates collagen-induced platelet aggregation via nuclear-factor-kappa-B (NF-κB) activation, Thromb. Res. 148 (2016) 15–22.
[31] X. Lan, J. Zhao, Y. Zhang, et al., Oxymatrine exerts organ- and tissue-protective effects by regulating inflammation, oxidative stress, apoptosis, and fibrosis: From bench to bedside, Pharmacol. Res. 151 (2020), 104541.
[32] M. Lu, X. Xiang, S. Xia, Potential signaling pathways involved in the clinical application of oxymatrine, Phytother Res. 30 (2016) 1104–1112.
[33] X. Wang, F. Chen, H. Shi, et al., Oxymatrine inhibits neuroinflammation byRegulating M1/M2 polarization in N9 microglia through the TLR4/NF-κB pathway, Int. Immunopharm. 100 (2021), 108139.
[34] N. Huang, M. Lou, H. Liu, et al., Identification of a potent small molecule capable of regulating polyploidization, megakaryocyte maturation, and platelet production, J. Hematol. Oncol. 9 (2016), 136.
[35] J.C. Stockert, A. Blázquez-Castro, R.W. Horobin, Identifying different types of chromatin using Giemsa staining, Methods Mol. Biol. 1094 (2014) 25–38.
[36] L. Wang, T. Zhang, S. Liu, et al., Discovery of a novel megakaryopoiesis enhancer, ingenol, promoting thrombopoiesis through PI3K-Akt signaling independent of thrombopoietin, Pharmacol. Res. 177 (2022), 106096.
[37] Y. Li, R. Li, Z. Feng, et al., Linagliptin regulates the mitochondrial respiratory reserve to alter platelet activation and arterial thrombosis, Front. Pharmacol. 11 (2020), 585612.
[38] K. Suzuki-Inoue, Y. Yatomi, N. Asazuma, et al., Rac, a small guanosine triphosphate-binding protein, and p21-activated kinase are activated during platelet spreading on collagen-coated surfaces: Roles of integrin $\alpha_2\beta_1$, Blood 98 (2001) 3708–3716.
[39] V.D. Hähnke, S. Kim, E.E. Bolton, PubChem chemical structure standardization, J. Cheminform. 10 (2018), 36.
[40] A. Forouzesh, S. Samadi Foroushani, F. Forouzesh, et al., Reliable target prediction of bioactive molecules based on chemical similarity without employing statistical methods, Front. Pharmacol. 10 (2019), 835.
[41] D. Szklarczyk, J.H. Morris, H. Cook, et al., The STRING database in 2017: Quality-controlled protein-protein association networks, made broadly accessible, Nucleic Acids Res. 45 (2017) D362–D368.
[42] D. Rossi, A. Guerrini, R. Bruni, et al., Trans-resveratrol in nutraceuticals: Issues in retail quality and effectiveness, Molecules 17 (2012) 12393–12405.
[43] P. Xiong, X. Huang, N. Ye, et al., Cytotoxicity of metal-based nanoparticles: From mechanisms and methods of evaluation to pathological manifestations, Adv. Sci. 9 (2022), e2106049.
[44] L. Hu, W. Zhang, Z. Xiang, et al., EloA promotes HEL polyploidization upon PMA stimulation through enhanced ERK1/2 activity, Platelets 33 (2022) 755–763.
[45] J. van Dijk, G. Bompard, J. Cau, et al., Microtubule polyglutamylation and acetylation drive microtubule dynamics critical for platelet formation, BMC Biol. 16 (2018), 116.
[46] K. Jimenez, V. Khare, R. Evstatiev, et al., Increased expression of HIF2α during iron deficiency-associated megakaryocytic differentiation, J. Thromb. Haemostasis 13 (2015) 1113–1127.
[47] S. De Botton, S. Sabri, E. Daugas, et al., Platelet formation is the consequence of caspase activation within megakaryocytes, Blood 100 (2002) 1310–1317.
[48] X. Zhang, W. Huang, M. Zhang, et al., Utility of mean platelet volume in differentiating intrahepatic cholangiocarcinoma from hepatocellular carcinoma, BMC Gastroenterol. 22 (2022), 288.
[49] K. Venkateswaran, A. Shrivastava, P.K. Agrawala, et al., Mitigation of radiation-induced hematopoietic injury by the polyphenolic acetate 7,8-diacetoxy-4-methylthiocoumarin in mice, Sci. Rep. 6 (2016), 37305.
[50] F. Milano, F. Merriam, I. Nicoud, et al., Notch-expanded murine hematopoietic stem and progenitor cells mitigate death from lethal radiation and convey immune tolerance in mismatched recipients, Stem Cells Transl. Med. 6 (2017) 566–575.
[51] C. Wang, B. Zhang, S. Wang, et al., Recombinant human thrombopoietin promotes hematopoietic reconstruction after severe whole body irradiation, Sci. Rep. 5 (2015), 12993.
[52] C. Short, H.K. Lim, J. Tan, et al., Targeting the spleen as an alternative site for hematopoiesis, Bioessays 41 (2019), e1800234.
[53] J.Y. Suen, B. Gardiner, S. Grimmond, et al., Profiling gene expression induced by protease-activated receptor 2 (PAR2) activation in human kidney cells, PLoS One 5 (2010), e13809.
[54] J. Shi, R. Tong, M. Zhou, et al., Circadian nuclear receptor Rev-erbalpha is expressed by platelets and potentiates platelet activation and thrombus formation, Eur. Heart J. 43 (2022) ehac544.3035.
[55] A. Morel, J. Rywaniak, M. Bijak, et al., Flow cytometric analysis reveals the high levels of platelet activation parameters in circulation of multiple sclerosis patients, Mol. Cell. Biochem. 430 (2017) 69–80.
[56] V.V. Inamdar, J.C. Kostyak, R. Badolia, et al., Impaired glycoprotein VI-mediated signaling and platelet functional responses in CD45 knockout mice, Thromb. Haemost. 119 (2019) 1321–1331.
[57] J. Bussel, D.M. Arnold, E. Grossbard, et al., Fostamatinib for the treatment of adult persistent and chronic immune thrombocytopenia: Results of two phase 3, randomized, placebo-controlled trials, Am. J. Hematol. 93 (2018) 921–930.
[58] E.M. Golebiewska, A.W. Poole, Platelet secretion: From haemostasis to wound healing and beyond, Blood Rev. 29 (2015) 153–162.
[59] P. Wojciechowski, K. Wilson, J. Nazir, et al., Efficacy and safety of avatrombopag in patients with chronic immune thrombocytopenia: A systematic literature review and network meta-analysis, Adv. Ther. 38 (2021) 3113–3128.
[60] S. Robinson, O. McGonigle, S. Volin, et al., Comprehensive look at blood transfusion utilization in total joint arthroplasty at a single academic medical center under a single surgeon, J. Blood Transfus. 2013 (2013), 983250.
[61] X. Jiang, Y. Sun, S. Yang, et al., Novel chemical-structure TPOR agonist, TMEA, promotes megakaryocytes differentiation and thrombopoiesis via mTOR and ERK signalings, Phytomedicine 110 (2023), 154637.
[62] S. van den Oudenrijn, M. Bruin, C.C. Folman, et al., Mutations in the thrombopoietin receptor, Mpl, in children with congenital amegakaryocytic thrombocytopenia, Br. J. Haematol. 110 (2000) 441–448.
[63] J.N. Poston, T.B. Gernsheimer, Glucocorticoids promote response to thrombopoietin-receptor agonists in refractory ITP: A case series, Int. J. Hematol. 110 (2019) 255–259.

[64] W. Liu, Z. Tan, Y. Zhao, et al., Panaxadiol saponin ameliorates ferroptosis in iron-overload aplastic anemia mice and Meg-01 cells by activating Nrf2/HO-1 and PI3K/AKT/mTOR signaling pathway, Int. Immunopharm. 118 (2023), 110131.
[65] R. Schwarzer, L. Laurien, M. Pasparakis, New insights into the regulation of apoptosis, necroptosis, and pyroptosis by receptor interacting protein kinase 1 and caspase-8, Curr. Opin. Cell Biol. 63 (2020) 186–193.
[66] O. Komolafe, S.P. Pereira, B.R. Davidson, et al., Serum C-reactive protein, procalcitonin, and lactate dehydrogenase for the diagnosis of pancreatic necrosis, Cochrane Database Syst. Rev. 4 (2017), CD012645.
[67] S. Van Wilpe, R. Koornstra, M. Den Brok, et al., Lactate dehydrogenase: A marker of diminished antitumor immunity, OncoImmunology 9 (2020), 1731942.
[68] M. Ogura, Y. Morishima, R. Ohno, et al., Establishment of a novel human megakaryoblastic leukemia cell line, MEG-01, with positive Philadelphia chromosome, Blood 66 (1985) 1384–1392.
[69] R. Alitalo, Induced differentiation of K562 leukemia cells: A model for studies of gene expression in early megakaryoblasts, Leuk. Res. 14 (1990) 501–514.
[70] V.K. Singh, T.M. Seed, Radiation countermeasures for hematopoietic acute radiation syndrome: Growth factors, cytokines and beyond, Int. J. Radiat. Biol. 97 (2021) 1526–1547.
[71] L.P. D'Atri, C.S. Rodríguez, C.P. Miguel, et al., Activation of toll-like receptors 2 and 4 on CD34$^+$ cells increases human megakaryo/thrombopoiesis induced by thrombopoietin, J. Thromb. Haemostasis 17 (2019) 2196–2210.
[72] M. Jayachandran, G.J. Brunn, K. Karnicki, et al., *In vivo* effects of lipopolysaccharide and TLR4 on platelet production and activity: Implications for thrombotic risk, J. Appl. Physiol. 102 (2007) 429–433.
[73] G. Andonegui, S.M. Kerfoot, K. McNagny, et al., Platelets express functional Toll-like receptor-4, Blood 106 (2005) 2417–2423.
[74] M. Yamamoto, S. Sato, H. Hemmi, et al., Role of adaptor TRIF in the MyD88-independent toll-like receptor signaling pathway, Science 301 (2003) 640–643.
[75] E. Kobatake, T. Kabuki, S-layer protein of *Lactobacillus helveticus* SBT2171 promotes human β-defensin 2 expression via TLR2-JNK signaling, Front. Microbiol. 10 (2019), 2414.
[76] W.J. Lu, K.H. Lin, M.J. Hsu, et al., Suppression of NF-κB signaling by andrographolide with a novel mechanism in human platelets: Regulatory roles of the p38 MAPK-hydroxyl radical-ERK2 cascade, Biochem. Pharmacol. 84 (2012) 914–924.
[77] L. Rivadeneyra, A. Carestia, J. Etulain, et al., Regulation of platelet responses triggered by Toll-like receptor 2 and 4 ligands is another non-genomic role of nuclear factor-kappaB, Thromb. Res. 133 (2014) 235–243.
[78] K. Kojok, A.E. El-Kadiry, Y. Merhi, Role of NF-κB in platelet function, Int. J. Mol. Sci. 20 (2019), 4185.
[79] L. Ou, A. Zhang, Y. Cheng, et al., The cGAS-STING pathway: A promising immunotherapy target, Front. Immunol. 12 (2021), 795048.
[80] G.N. Barber, Sting: Infection, inflammation and cancer, Nat. Rev. Immunol. 15 (2015) 760–770.
[81] Y. Zhang, R. Yan, Y. Hu, Oxymatrine inhibits lipopolysaccharide-induced inflammation by down-regulating Toll-like receptor 4/nuclear factor-kappa B in macrophages, Can. J. Physiol. Pharmacol. 93 (2015) 253–260.